A Time Dependent Approach for Removing the Cell Boundary Error in Elliptic Homogenization Problems

Doghonay Arjmand[a,*], Olof Runborg[b]

[a] *Division of Scientific Computing, Department of Information Technology, Uppsala University, Sweden*
[b] *Department of Mathematics and Swedish e-Science Research Center (SeRc), Royal Institute of Technology (KTH), Sweden*

Abstract

This paper concerns the cell-boundary error present in multiscale algorithms for elliptic homogenization problems. Typical multiscale methods have two essential components: a macro and a micro model. The micro model is used to upscale parameter values which are missing in the macro model. To solve the micro model, boundary conditions are required on the boundary of the microscopic domain. Imposing a naive boundary condition leads to $O(\varepsilon/\eta)$ error in the computation, where ε is the size of the microscopic variations in the media and η is the size of the micro-domain. The removal of this error in modern multiscale algorithms still remains an important open problem. In this paper, we present a time-dependent approach which is general in terms of dimension. We provide a theorem which shows that we have arbitrarily high order convergence rates in terms of ε/η in the periodic setting. Additionally, we present numerical evidence showing that the method improves the $O(\varepsilon/\eta)$ error to $O(\varepsilon)$ in general non-periodic media.

Keywords: Multiscale Problems, Homogenization, Elliptic PDEs

1. Introduction

In the present paper, we are interested in developing a multiscale method for the numerical homogenization of multiscale elliptic PDEs in divergence form:

$$\begin{aligned} -\nabla\cdot(A^\varepsilon(\boldsymbol{x})\nabla u^\varepsilon(\boldsymbol{x})) &= f(\boldsymbol{x}) \quad \text{in} \quad \Omega, \\ u^\varepsilon(\boldsymbol{x}) &= 0 \quad \text{on} \quad \partial\Omega, \end{aligned} \tag{1}$$

where Ω is an open bounded set in $\mathbb{R}^d$ with $|\Omega| = O(1)$, $\varepsilon \ll 1$ and A^ε is a symmetric, uniformly elliptic and bounded, matrix function in $\mathbb{R}^{d\times d}$ such that for every $\zeta \in \mathbb{R}^d$

$$c_1|\zeta|^2 \leq \sup_{\boldsymbol{x}\in\Omega} \zeta^T A^\varepsilon(\boldsymbol{x})\zeta \leq c_2|\zeta|^2. \tag{2}$$

*Corresponding author
Email addresses: doghonay.arjmand@it.uu.se (Doghonay Arjmand), olofr@kth.se (Olof Runborg)

The multiscale method does not assume any knowledge about the exact form of $A^\varepsilon(\boldsymbol{x})$. However, for the sake of comparison with known analytical results, the numerical examples and theoretical claims in this paper are given mainly in two settings: (a) for periodic media where $A^\varepsilon(\boldsymbol{x}) = A(\boldsymbol{x}/\varepsilon)$ and A is a periodic matrix function in the d-dimensional unit cube $Y := (0,1]^d$, and (b) for locally-periodic media where $A^\varepsilon(\boldsymbol{x}) = A(\boldsymbol{x}, \boldsymbol{x}/\varepsilon)$ and $A(x,\cdot)$ is Y-periodic and $A_{ij} \in C^\infty(\overline{\Omega} \times Y)$. The smoothness assumptions are only to simplify the analysis and the method performs equally well under weaker assumptions, e.g. $\partial_x^k A_{ij} \in C(\overline{\Omega}; L^\infty(Y))$ at least for all $k \leq 2$.

The term numerical homogenization is used to mean approximating the homogenized solutions of multiscale PDEs without resolving the small scales over the entire domain. Equation (1) models, for instance, steady heat conduction in heterogeneous media, where ε stands for the length-scale of the microscopic variations in the media. A direct numerical simulation of (1) leads to $O(\varepsilon^{-d})$ degrees of freedom which can not be handled even by the best available computers if ε is very small. The aim of homogenization is to describe the macroscopic behaviour of the heterogeneous system (1). The idea behind homogenization theory is to mix the heterogeneities of the media infinitely to obtain a homogeneous system which is no more dependent on ε. Traditional numerical techniques will then be amenable for solving the resulting homogenized system.

From a mathematical point of view, the homogenization of equation (1), for purely periodic or a more realistic locally periodic coefficients is well-known, see e.g. [1, 2, 3]. In the periodic setting, as $\varepsilon \to 0$, the solution to (1) tends to the homogenized solution $u^0(\boldsymbol{x})$ which satisfies

$$\begin{array}{c} -\nabla \cdot \left(A^0 \nabla u^0(\boldsymbol{x})\right) = f(\boldsymbol{x}) \quad \text{in} \quad \Omega, \\ u^0(\boldsymbol{x}) = 0 \quad \text{on} \quad \partial\Omega. \end{array} \tag{3}$$

Here the effective conductivity A^0 is a constant matrix given by

$$A^0_{ij} = \int_Y \left(A_{ij}(\boldsymbol{y}) + \sum_{k=1}^{d} A_{ik} \nabla_{\boldsymbol{y}_k} \chi_j(\boldsymbol{y}) \right) \, d\boldsymbol{y}, \tag{4}$$

where the cell solutions $\boldsymbol{\chi} = \{\chi_i\}_{i=1}^d$ are Y-periodic functions that solve the following periodic problems:

$$\begin{array}{l} -\nabla \cdot (A(\boldsymbol{y}) \nabla \chi_i(\boldsymbol{y})) = \nabla \cdot A(\boldsymbol{y}) \boldsymbol{e}_i \quad \text{in} \quad Y, \\ \chi_i(\boldsymbol{y}) \text{ is } Y\text{-periodic}, \quad \int_Y \chi_i(\mathbf{s}) \, d\mathbf{s} = 0, \end{array} \tag{5}$$

where $\{\boldsymbol{e}_i\}_{i=1}^d$ are the canonical basis vectors in $\mathbb{R}^d$. The above formula is valid for periodic and, with a slight modification, for locally-periodic media. In more general settings, on the other hand, finding the limiting behaviour of (1) is difficult and often impossible through existing theory of homogenization.

Numerical homogenization is indispensible in cases when homogenization theory is not adequate for finding the effective parameters of the media. From a numerical homogenization point of view, the focus is to develop computationally cheap methods which are potentially applicable to general settings, where the coefficient $A^\varepsilon(\boldsymbol{x})$ is allowed to have more general oscillations/variations in fast and slow scales. Keeping the generality of the main physical model (1) in mind, it is important then to develop a method which does not assume any knowledge about the form of the coefficient $A^\varepsilon(\boldsymbol{x})$, and at the same time performs optimally when applied to periodic and locally-periodic media.

1.1. The heterogeneous multiscale methods

E and Engquist [4], proposed the Heterogeneous Multiscale Methods (HMM) framework as a general methodology for capturing the global/average behaviour of multiscale and possibly multi-physics problems. HMM is often very useful when we have a full description of the microscopic model. The idea is to avoid resolving the small scale details all over the domain, at the expense of targeting only an average behaviour of the system. Multiscale PDEs such as (1) is whithin the application areas of HMM. In a typical HMM-based multiscale method, one starts by assuming a macroscopic model with some unknown data. The macroscopic model is discretized through standard finite difference (FD) or finite element methods (FEM) on a coarse mesh. Therefore, one needs the missing data on discrete points of the macro grid. These unknown data have local origin, which in turn is extracted from microscopic simulations performed over boxes of size $\eta = O(\varepsilon)$, where ε represents the size of the small scale in the problem. Already here, we see that HMM exploits the scale separation featured in the main problem (1). In other words, since $\varepsilon \ll 1$, we can set $\eta = O(\varepsilon)$ and therefore the computational cost of the micro simulations will not increase by decreasing ε. It is important to note that the microscopic simulations should be consistent with the current macroscopic data. This is achieved by restricting the microscopic simulations by the coarse-scale information. The overall computational cost of this HMM-based algorithm will then be NC_{micro}, where N is the number of macro grid points and C_{micro} is the cost of performing a single micro simulation, which can be made essentially independent of ε by using high order methods, cf [5]. For other approaches to decrease the computational burden in linear and quasi-linear elliptic multiscale PDEs see e.g. [6, 7, 8].

Now assume that $\Omega = (0,1)^d$. The macro model for a standard HMM-type algorithm for problem (1) is

$$\text{Macro Problem:} \quad \begin{array}{c} -\nabla \cdot \boldsymbol{F}(\boldsymbol{x}, \nabla U) = f(\boldsymbol{x}) \text{ in } \Omega \\ U = 0 \text{ on } \partial\Omega. \end{array} \tag{6}$$

Here U represents the solution of the macro problem and the flux $\boldsymbol{F} = (F^1, F^2, \ldots, F^d)$ is an unknown parameter which will be extracted from micro simulations. A simple finite difference discretization (in two dimensions) of the macro problem (6) on the grid

$$\{\boldsymbol{x}_{i,j} = (iH, jH), \quad i,j = 0, \ldots, N, \quad NH = 1\}$$

yields

$$\text{Macro Solver:} \quad -\left(\frac{F^1_{i+\frac{1}{2},j} - F^1_{i-\frac{1}{2},j}}{H} + \frac{F^2_{i,j+\frac{1}{2}} - F^2_{i,j-\frac{1}{2}}}{H} \right) = f_{ij}, \tag{7}$$

where H stands for the macro stepsize. Next, to compute the unknown $\boldsymbol{F}_{i+1/2,j}$, one solves (1) over micro boxes $\Omega_{i+1/2,j}$ of size $\eta = O(\varepsilon)$, centered at $\boldsymbol{x}_{i+1/2,j}$. Furthermore, the coarse scale solutions $U_{i,j}$ are used as boundary data for the micro problem, which reads

$$\text{Micro Problem:} \quad \begin{array}{ccc} -\nabla \cdot (A^\varepsilon(\boldsymbol{x}) \nabla w^{\varepsilon,\eta}(\boldsymbol{x})) = 0 & \text{in} & \Omega_{i+1/2,j}, \\ w^{\varepsilon,\eta}(\boldsymbol{x}) = \hat{u}(\boldsymbol{x}), & \text{on} & \partial\Omega_{i+1/2,j}. \end{array} \tag{8}$$

Here $\hat{u}(\boldsymbol{x}) := \Pi_1(U_{m,l})(\boldsymbol{x})$ where Π_1 is a linear interpolation operator which, in two dimensions, interpolates few nearest coarse scale solutions $\{U_{m,l}\}$, with $m = i, i+1$ and

$\ell = j-1, j, j+1$. The last step of the HMM algorithm is to average the microscopic flux $\boldsymbol{F}^\varepsilon := A^\varepsilon \nabla w^{\varepsilon,\eta}$ over the micro domain. This can be done much more accurately if one uses a weighted average of $\boldsymbol{F}^\varepsilon$. Hence we introduce the kernel space $\mathbb{K}^{p,q}$ which consists of kernels K, compactly supported in $[-1/2, 1/2]$, with $K^{(q+1)} \in BV(\mathbb{R})$, and p vanishing moments:

$$\int_{\mathbb{R}} K(x) x^r dx = \begin{cases} 1, & r = 0. \\ 0, & 1 \le r \le p. \end{cases}$$

Here $K^{(q+1)}$ stands for the $(q+1)$th weak derivative and $BV(\mathbb{R})$ is the space of functions of bounded variations. Note that, a constant kernel $K = 1$ in $[-1/2, 1/2]$ has $q = -1$. We use the scaling $K_\eta(x) = \dfrac{1}{\eta} K(\dfrac{x}{\eta})$ to shrink the compact support of the kernel to the interval $[-\eta/2, \eta/2]$, and we compute the HMM flux $\boldsymbol{F}$ as follows

$$\text{Upscaling: } \boldsymbol{F} = \int_{\Omega_{i+1/2,j}} K_\eta(\boldsymbol{x} - \boldsymbol{x}_{i+\frac{1}{2},j}) A^\varepsilon(\boldsymbol{x}) \nabla w^{\varepsilon,\eta}(\boldsymbol{x})\, d\boldsymbol{x}. \tag{9}$$

In d dimensions, the kernel K_η is defined as

$$K_\eta(\boldsymbol{x}) := K_\eta(\boldsymbol{x}_1) \cdots K_\eta(\boldsymbol{x}_d).$$

The HMM flux $\boldsymbol{F}_{i+1/2,j}$ approximates the homogenized flux $\hat{\boldsymbol{F}}$ defined as

$$\hat{\boldsymbol{F}} = A^0 \nabla \hat{u}, \tag{10}$$

where $\hat{u}$ is given in (8). For an analysis of the FEM version of the HMM for elliptic problems we refer the reader to [9], see also [10] for a fully discrete analysis.

To explain the role of linear initial data for the micro model (8), suppose $\hat{u} = x_i$ and let $w^{\varepsilon,\eta} = \hat{u} + v^{\varepsilon,\eta}$, then $-\nabla \cdot A^\varepsilon \nabla v^{\varepsilon,\eta} = \nabla \cdot A^\varepsilon \boldsymbol{e}_i$. Note the similarity between this equation and (5). From (9) we get $F^j = \int_{\Omega_{i+1/2,j}} K_\eta(\boldsymbol{x} - \boldsymbol{x}_{i+1/2})(A^\varepsilon_{ij} + \boldsymbol{e}_j^T A^\varepsilon \nabla v^{\varepsilon,\eta})\, d\boldsymbol{x}$ which approximates the homogenized flux $\hat{\boldsymbol{F}}$ where A^0 is given in (4).

1.2. Errors in the HMM micro problem

In this part, we discuss the sources of the HMM error in the periodic case, defined as

$$E_{HMM} = \left| \boldsymbol{F} - \hat{\boldsymbol{F}} \right|,$$

where $\boldsymbol{F}$ and $\hat{\boldsymbol{F}}$ are given in (9) and (10) respectively. We divide the HMM error into three parts:

- Discretization error when solving the micro problem (8) and approximating the integral (9) numerically.
- Averaging/filtering error introduced by the averaging kernel in (9). This error originates from the difference between the exact integral (9) and the average of the integrand in the limit when $\varepsilon/\eta \longrightarrow 0$.
- A first order (in ε/η) error due to boundary conditions, in the micro problem, which are $O(\varepsilon)$ away from the exact value. We will focus on the cell-boundary error in section 2.

The first two sources of errors can be made as small as we like by using high-order solvers for the micro model, a high order quadrature rule, and by using averaging operators with high q, p. However the error due to the boundary will eventually dominate all other errors. In the last decade, the removal or reduction of the cell boundary error has been the subject of active research. The performance of simple Dirichlet, Neuman and periodic boundary conditions were tested numerically in [11]. The numerical results presented in [11] showed that the convergence rate for these type of classical boundary conditions is $O(\varepsilon/\eta)$ and that in most cases a simple periodic boundary condition performs better than others with a smaller prefactor. Another approach, based on oversampling, for removing only the first-order cell boundary error was proposed in [12]. These approaches used the same elliptic problem as the micro scale model but they improved only the prefactor in the first order error. In [13], an L^2 projection of the solution u^ε of (1) into a finite dimensional space incorporating the coarse features of u^ε was considered. The authors showed linear convergence rate, in terms of the coarse mesh size H, for the difference between the exact u^ε and the projected solution. The projected solution, however, is $O(\varepsilon)$ away from the homogenized solution, see [14].

Another class of techniques for boundary error reduction is based on modifying the micro problem such that the new micro solutions are less influenced by the boundary error. The filtering technique from [15] is within this class. The filter is used already in the definition of the micro problem as well as in a complementary integral boundary condition involving the gradient of the micro problem. To be more precise the authors considered the equation

$$\text{Micro Problem:} \quad \begin{array}{c} -\nabla \cdot \left(K_\eta * \left(A^\varepsilon \nabla w^{\varepsilon,\eta} + \lambda\right)(\boldsymbol{x})\right) = 0 \quad \text{in} \quad \Omega_\eta, \\ \int_{\Omega_\eta} K_\eta(\boldsymbol{x}) \nabla w^{\varepsilon,\eta}(\boldsymbol{x})\, d\boldsymbol{x} = \nabla \hat{u}, \end{array} \tag{11}$$

where $\lambda \in \mathbb{R}^n$ is the vector of Lagrange multipliers for the integral constraint in (11), and Ω_η represents the micro domain. Although this method performed optimally in one-dimension, in higher dimensions (even in the periodic setting) the approach led to only second order convergence rate in ε/η. A different approach was proposed in [16]. This technique used a zero order regularization term in the definition of the micro problem. The motivation behind this strategy is that for the modified micro problem the decay of the corresponding Green's function for the elliptic problem is exponentially fast. Hence the effect of boundary data on the interior solution reduces substantially. Mathematically speaking, the micro problem is given by

$$\text{Micro Problem:} \quad \delta_{\eta,\varepsilon} w^{\varepsilon,\eta}(\boldsymbol{x}) - \nabla \cdot \left(A^\varepsilon(\boldsymbol{x}) \nabla w^{\varepsilon,\eta}(\boldsymbol{x})\right) = 0 \quad \text{in} \quad \Omega_\eta, \tag{12}$$

together with a suitable boundary condition (in practice any well-posed boundary condition). With an appropriate choice of the parameter $\delta_{\eta,\varepsilon}$ depending on η and ε, one can obtain fourth order convergence $O((\varepsilon/\eta)^4)$ in the periodic setting even in higher dimensions. Recently, it was shown that the $O((\varepsilon/\eta)^4)$ error can be further improved (in periodic media) using extrapolation, see [17]. However, to achieve this, the micro problem (12) must be solved over larger and larger domains. Another strategy which eliminates the boundary error in the framework of multiscale finite element methods (MsFEM) is proposed in [18].

In the present work, we introduce a strategy based on the HMM which, in periodic media, improves the convergence rate up to $O((\varepsilon/\eta)^{q+2})$ for arbitrary $q > 0$, upon using

a kernel $K \in K^{p,q}$. Unlike [17] the computational cost remains the same for all q. We present also numerical evidence which show that in general non-periodic media the error becomes $O(\varepsilon^k + (\varepsilon/\eta)^{q+2})$ if $p > 1$. Here k can be equal to $k = 1$ or $k = 2$ depending on the dimension. The $O(\varepsilon)$ term is not harmful as this is a typical error tolerance we are interested in. The reason is that the homogenized solution solving (3) is already $O(\varepsilon)$ away from the exact solution u^ε solving (1). The strategy described here can be easily used in the framework of MsFEM, see e.g. [19, 20, 21].

1.3. Contents

This paper is organized as follows. In section 2, we motivate the cell-boundary error by considering a micro problem with Dirichlet boundary conditions. Section 3 is devoted to the study of micro problems involving integral conditions in one and two dimensions. The main part of the paper is section 4, where we introduce our strategy to reduce the boundary error. Finally, we conclude our paper with numerical examples supporting our theoretical results.

2. Boundary and averaging errors

In this section, we consider a micro problem with Dirichlet boundary conditions as a representative of classical boundary conditions such as Neuman and periodic BCs. We ignore the discretization error and divide the HMM error into two parts: boundary and averaging errors. In particular, we will show that although the averaging error can be made arbitrarily small, the overall error is dominated by the boundary error. To fix ideas, consider the micro problem (8) in d dimensions, where $A^\varepsilon(\boldsymbol{x}) = A(\boldsymbol{x}/\varepsilon)$ and A is Y-periodic. The boundary data is again given by the linear macroscopic function $\hat{u}(\boldsymbol{x}) = \mathbf{s} \cdot \boldsymbol{x}$, where $\mathbf{s} := \nabla \hat{u} \in \mathbb{R}^d$ is the slope vector. Moreover, we assume that the micro problem (8) is posed on the micro domain $\Omega_\eta := [-\eta/2, \eta/2]^d$ so that

$$\begin{aligned} -\nabla \cdot (A(\boldsymbol{x}/\varepsilon)\nabla w^{\varepsilon,\eta}(\boldsymbol{x})) &= 0, \quad \text{in } \Omega_\eta \\ w^{\varepsilon,\eta}(\boldsymbol{x}) &= \hat{u}(\boldsymbol{x}), \quad \text{on } \partial\Omega_\eta. \end{aligned} \tag{13}$$

Next we define the *infinite domain solution* $w^{\varepsilon,\infty}$ as

$$w^{\varepsilon,\infty}(\boldsymbol{x}) := \hat{u}(\boldsymbol{x}) + \varepsilon \boldsymbol{\chi}(\boldsymbol{x}/\varepsilon) \cdot \nabla \hat{u}(\boldsymbol{x}), \tag{14}$$

where $\boldsymbol{\chi} = \{\chi_m\}_{m=1}^d$ are the solutions of the cell problem (5). The infinite domain solution $w^{\varepsilon,\infty}$ can be interpreted as the limit as $\eta \longrightarrow \infty$ of $w^{\varepsilon,\eta}$ for a fixed ε. By (5), we have

$$-\nabla \cdot (A(\boldsymbol{x}/\varepsilon)\nabla w^{\varepsilon,\infty}) = 0, \quad \text{in } \Omega_\eta.$$

Let $\theta^{\varepsilon,\eta} := w^{\varepsilon,\eta} - w^{\varepsilon,\infty}$. The term $\theta^{\varepsilon,\eta}$ is nonzero because of the mismatch due to the difference at the boundary of the micro problem. The HMM error can now be split as

$$\begin{aligned} \left| \boldsymbol{F} - \hat{\boldsymbol{F}} \right| &:= \left| \int_{\Omega_\eta} K_\eta(\boldsymbol{x}) A(\boldsymbol{x}/\varepsilon) \nabla w^{\varepsilon,\eta}(\boldsymbol{x}) \, d\boldsymbol{x} - A^0 \nabla \hat{u} \right| \\ &\leq \underbrace{\left| \int_{\Omega_\eta} K_\eta(\boldsymbol{x}) A(\boldsymbol{x}/\varepsilon) \nabla \theta^{\varepsilon,\eta} \, d\boldsymbol{x} \right|}_{\text{Boundary error}} + \underbrace{\left| \int_{\Omega_\eta} K_\eta(\boldsymbol{x}) A(\boldsymbol{x}/\varepsilon) \nabla w^{\varepsilon,\infty}(\boldsymbol{x}) \, d\boldsymbol{x} - A^0 \nabla \hat{u} \right|}_{\text{Averaging error}}. \end{aligned}$$

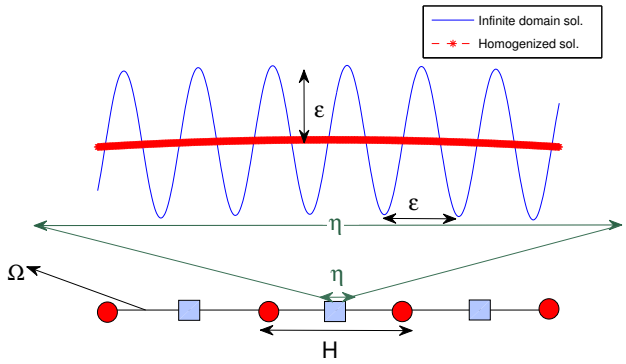

Figure 1: HMM discretization and solutions. Bottom: The physical domain Ω. Top: zoom of solutions in micro box. The circles are the macro discretization points and the rectangular boxes are the micro domains. The homogenized solution is $O(\varepsilon)$ away from the infinite domain solution on the boundary of the microscopic domain.

In the remainder of this section we will show that if $K \in \mathbb{K}^{p,q}$:

$$\left| \int_{\Omega_\eta} K_\eta(\boldsymbol{x}) A(\boldsymbol{x}/\varepsilon) \nabla \theta^\varepsilon \, d\boldsymbol{x} \right| \leq C \left(\frac{\varepsilon}{\eta} \right), \quad \left| \int_{\Omega_\eta} K_\eta(\boldsymbol{x}) A(\boldsymbol{x}/\varepsilon) \nabla w^{\varepsilon,\infty} \, d\boldsymbol{x} - A^0 \nabla \hat{u} \right| \leq C \left(\frac{\varepsilon}{\eta} \right)^{q+2}.$$

This motivates that the boundary error dominates the HMM error and, in contrast to the averaging error, one can not remove this error by taking a kernel with higher q, i.e., better regularity properties. Moreover, in order for the HMM flux to approximate the homogenized flux accurately, the micro solution $w^{\varepsilon,\eta}$ must be very close to the infinite domain solution $w^{\varepsilon,\infty}$. We remark also that although the results will be proved for the Dirichlet case, the final claims hold true also for the Neuman and periodic BCs. In the rest of this section we treat the boundary and the averaging errors separately.

2.1. Boundary error

In this section, we state a theorem which shows that the boundary error is of first order in ε/η which can not be improved even for smooth coefficients $A \in C^\infty(Y)$. To simplify the analysis, we assume that $\chi_i \in W^{1,\infty}(Y)$ which would then require more regularity on the coefficient A. For this, it is sufficient to assume $A \in W^{1,k}(Y)$ with $k > d$ (see [22], condition 15.1). See also Remark 1 for additional comments on regularity.

Theorem 1. *Suppose that $A \in W^{1,k}(Y)$ for $k > d$ so that $\chi_i \in W^{1,\infty}(Y)$. Let $\theta^{\varepsilon,\eta} := w^{\varepsilon,\eta} - w^{\varepsilon,\infty}$, where $w^{\varepsilon,\eta}$ is the solution of (13) and let $w^{\varepsilon,\infty}$ be given as in (14) with $\hat{u}(x) = \mathbf{s} \cdot \boldsymbol{x}$. Then*

$$\|\nabla \theta^{\varepsilon,\eta}\|_{L^2(\Omega_\eta)} \leq C \left(\frac{\varepsilon}{\eta} \right)^{1/2} \|\nabla \hat{u}\|_{L^2(\Omega_\eta)}, \tag{15}$$

and if $K \in \mathbb{K}^{p,q}$*, with* $q \geq 0$*,*

$$\left| \int_{\Omega_\eta} K_\eta(\boldsymbol{x}) A(\boldsymbol{x}/\varepsilon) \nabla \theta^{\varepsilon,\eta} \, d\boldsymbol{x} \right| \leq C \frac{\varepsilon}{\eta} \left| \mathbf{s} \right|_\infty , \tag{16}$$

where $|\mathbf{s}|_\infty = \max_j |s_j|$ *and* C *is independent of* ε, η *but may depend on* A *and* K*.*

Proof. The inequality (15) is stated in [9] (estimate 3.9) but detailed ideas which cover more general domains (not only rectangular) can be found e.g. in [1, 2] under the assumption that $\chi_i \in W^{1,\infty}(Y)$. To prove (16) we first write $\theta^{\varepsilon,\eta} = \sum_{\ell=1}^d \theta_\ell^{\varepsilon,\eta} s_\ell$, where $\theta_\ell^{\varepsilon,\eta}$ solves

$$\begin{aligned} -\nabla \cdot (A(\boldsymbol{x}/\varepsilon) \nabla \theta_\ell^{\varepsilon,\eta}(\boldsymbol{x})) = 0, \quad & \text{in } \Omega_\eta, \\ \theta_\ell^{\varepsilon,\eta}(\boldsymbol{x}) = \phi_\ell^\varepsilon(\boldsymbol{x}), \quad & \text{on } \partial\Omega_\eta, \end{aligned} \tag{17}$$

with $\phi_\ell^\varepsilon(\boldsymbol{x}) = -\varepsilon \boldsymbol{\chi}_\ell(\boldsymbol{x}/\varepsilon)$. Since $A \nabla \theta^{\varepsilon,\eta}(\boldsymbol{x}) \in \mathbb{R}^d$ for all $\boldsymbol{x} \in \Omega_\eta$, it suffices to show that (16) holds componentwise. For this let $\psi(\boldsymbol{x}) = \boldsymbol{x}_m$, and denote the canonical basis vector in the mth direction by $\boldsymbol{e}_m$. Then we can write the mth component of the error as

$$\begin{aligned} E_m &:= \boldsymbol{e}_m \cdot \int_{\Omega_\eta} K_\eta(\boldsymbol{x}) A(\boldsymbol{x}/\varepsilon) \nabla \theta^{\varepsilon,\eta} \, d\boldsymbol{x} = \sum_{\ell=1}^d s_\ell \int_{\Omega_\eta} K_\eta(\boldsymbol{x}) \boldsymbol{e}_m \cdot A(\boldsymbol{x}/\varepsilon) \nabla \theta_\ell^{\varepsilon,\eta} \, d\boldsymbol{x} = \\ &= \sum_{\ell=1}^d s_\ell \int_{\Omega_\eta} K_\eta(\boldsymbol{x}) \nabla \psi(\boldsymbol{x}) \cdot A(\boldsymbol{x}/\varepsilon) \nabla \theta_\ell^{\varepsilon,\eta} \, d\boldsymbol{x} \\ &= \sum_{\ell=1}^d s_\ell \left(\int_{\Omega_\eta} K_\eta(\boldsymbol{x}) \nabla \left(\psi - \phi_m^\varepsilon\right) \cdot A(\boldsymbol{x}/\varepsilon) \nabla \theta_\ell^{\varepsilon,\eta} \, d\boldsymbol{x} + \int_{\Omega_\eta} K_\eta(\boldsymbol{x}) \nabla \phi_m^\varepsilon(\boldsymbol{x}) \cdot A(\boldsymbol{x}/\varepsilon) \nabla \theta_\ell^{\varepsilon,\eta} \, d\boldsymbol{x} \right) \\ &= -\left(\sum_{\ell=1}^d s_\ell \int_{\Omega_\eta} \theta_\ell^{\varepsilon,\eta} \nabla K_\eta(\boldsymbol{x}) \cdot A(\boldsymbol{x}/\varepsilon) \nabla \left(\psi - \phi_m^\varepsilon\right) \, d\boldsymbol{x} \right) - \int_{\Omega_\eta} \phi_m^\varepsilon(\boldsymbol{x}) \nabla K_\eta(\boldsymbol{x}) \cdot A(\boldsymbol{x}/\varepsilon) \nabla \theta^{\varepsilon,\eta} \, d\boldsymbol{x}. \end{aligned}$$

In the last step we used (17) and the fact that by (5),

$$\nabla \cdot (A(x/\varepsilon) \nabla \left(\phi_m^\varepsilon(x) - \psi(x)\right)) = 0, \quad \text{in } \Omega_\eta.$$

Hence,

$$\begin{aligned} |E_m| &\leq C \left(|\mathbf{s}|_\infty \max_\ell \|\theta_\ell^{\varepsilon,\eta} \nabla K_\eta\|_{L^2(\Omega_\eta)} \|\nabla \left(\psi - \phi_m^\varepsilon\right)\|_{L^2(\Omega_\eta)} + \|\phi_m^\varepsilon \nabla K_\eta\|_{L^2(\Omega_\eta)} \|\nabla \theta^{\varepsilon,\eta}\|_{L^2(\Omega_\eta)} \right) \\ &\leq C \left(|\mathbf{s}|_\infty \max_\ell \|\theta_\ell^{\varepsilon,\eta} \nabla K_\eta\|_{L^\infty(\Omega_\eta)} \|\nabla \left(\psi - \phi_m^\varepsilon\right)\|_{L^\infty(\Omega_\eta)} \eta^d + \|\phi_m^\varepsilon \nabla K_\eta\|_{L^\infty(\Omega_\eta)} \|\nabla \theta^{\varepsilon,\eta}\|_{L^2(\Omega_\eta)} \eta^{d/2} \right). \end{aligned}$$

For the kernel we have $\|\nabla K_\eta\|_{L^\infty(\Omega_\eta)} \leq C \eta^{-d-1}$, and by the maximum principle

$$\sup_{x \in \Omega_\eta} |\theta_\ell^{\varepsilon,\eta}| \leq \sup_{x \in \partial\Omega_\eta} |\theta_\ell^{\varepsilon,\eta}| = \sup_{x \in \partial\Omega_\eta} |\phi_\ell^\varepsilon| \leq \sup_{x \in \Omega_\eta} |\phi_\ell^\varepsilon| \leq C\varepsilon \|\chi_\ell\|_{L^\infty(\Omega_\eta)}.$$

Also note that by the assumption $\chi_m \in W^{1,\infty}(Y)$, we have $\|\nabla \left(\psi - \phi_m^\varepsilon\right)\|_{L^\infty(\Omega_\eta)} \leq C$. This gives us

$$\begin{aligned} |E_m| &\leq C \left(\frac{\varepsilon}{\eta^{d+1}} \eta^d |\mathbf{s}|_\infty + \frac{\varepsilon}{\eta^{d+1}} \|\nabla \theta^{\varepsilon,\eta}\|_{L^2(\Omega_\eta)} \eta^{d/2} \right) \\ &\leq C \left(\frac{\varepsilon}{\eta} |\mathbf{s}|_\infty + \frac{\varepsilon}{\eta} \|\nabla \theta^{\varepsilon,\eta}\|_{L^2(\Omega_\eta)} \eta^{-d/2} \right). \end{aligned}$$

Finally by (15),

$$\|\nabla\theta^{\varepsilon,\eta}\|_{L^2(\Omega_\eta)} \leq C\sqrt{\varepsilon\eta^{d-1}}|\mathbf{s}|_\infty.$$

This finishes the proof. □

Remark 1. *In fact it is sufficient to assume that $\chi_i \in W^{1,2}(Y)\cap L^\infty(Y)$ for an alternative proof of the Theorem 1. To see this first note that $\|\nabla\left(\psi-\phi_m^\varepsilon\right)\|_{L^2(\Omega_\eta)} \leq C_d\eta^{d/2}$ and $\|\phi_m^\varepsilon\nabla K_\eta\|_{L^2(\Omega_\eta)} \leq C\varepsilon\eta^{d/2}/\eta^{d+1}$ can be achieved directly if $\chi_m \in W^{1,2}(Y)$. Moreover, the fact that our micro-domains are rectangular together with the condition $\chi_m \in W^{1,2}(Y)$ are sufficient to carry out a similar proof as in [2] to show that* (15) *holds. Note that the condition $\chi_i \in L^\infty(Y)$ is needed only after the maximum principle is applied.*

To show that the inequality (16) is sharp, we consider the problem (17) in one dimension. The solution $\theta^{\varepsilon,\eta}$ can be explicitely written as

$$\theta^{\varepsilon,\eta}(x) = C_1\int_{-\eta/2}^{x} A^{-1}(z/\varepsilon)dz + C_2,$$

where

$$C_1 = -\left(\frac{\varepsilon}{\eta}\right) s\frac{\chi(\frac{\eta}{2\varepsilon}) - \chi(-\frac{\eta}{2\varepsilon})}{\frac{1}{\eta}\int_{-\eta/2}^{\eta/2} A^{-1}(\zeta/\varepsilon)d\zeta}, \quad \text{and} \quad C_2 = -\varepsilon s\chi\left(-\frac{\eta}{2\varepsilon}\right).$$

Therefore,

$$\begin{aligned}\int_{\Omega_\eta} K_\eta(x)A(x/\varepsilon)\partial_x\theta^{\varepsilon,\eta}(x)dx = C_1 &= -\left(\frac{\varepsilon}{\eta}\right) s\frac{\chi(\frac{\eta}{2\varepsilon}) - \chi(-\frac{\eta}{2\varepsilon})}{\frac{1}{\eta}\int_{-\eta/2}^{\eta/2} A^{-1}(s/\varepsilon)ds} \\ &= -\left(\frac{\varepsilon}{\eta}\right) s\frac{\chi(\frac{\eta}{2\varepsilon}) - \chi(-\frac{\eta}{2\varepsilon})}{\frac{1}{A^0} + C\frac{\varepsilon}{\eta}} = O\left(\frac{\varepsilon}{\eta}\right),\end{aligned}$$

where we used the fact that, in one dimension, the homogenized coefficient A^0 is given by

$$A^0 = \left(\int_0^1 A^{-1}(y)dy\right)^{-1}.$$

Remark 2. *For the periodic BCs where $w^{\varepsilon,\eta} - sx$ is η-periodic, we obtain the same C_1 as the Dirichlet case. Moreover, for the Neuman boundary condition*

$$A(\pm\frac{\eta}{2\varepsilon})\partial_x w^{\varepsilon,\eta}(\pm\frac{\eta}{2}) = s\left(\int_{-\eta/2}^{\eta/2} A^{-1}(\zeta/\varepsilon)d\zeta\right)^{-1},$$

we have

$$C_1 = s\left(\left(\int_{-\eta/2}^{\eta/2} A^{-1}(\zeta/\varepsilon)d\zeta\right)^{-1} - A^0\right) = O\left(\frac{\varepsilon}{\eta}\right).$$

To ensure uniqueness of the solutions to the periodic and Neuman problems, one needs the condition

$$\int_{-\eta/2}^{\eta/2} w^{\varepsilon,\eta}\,dx = sx.$$

We note here that the inequality (16) is sharp in higher dimensions as well; see the numerical results in [11]. As we see in the analysis above, the first order error $O(\varepsilon/\eta)$ in the flux approximation, originates from the $O(\varepsilon)$ difference between $w^{\varepsilon,\eta}$ and $w^{\varepsilon,\infty}$ on the boundary of the micro domain. To approximate the homogenized flux with high accuracy one needs to impose a boundary condition which ideally matches the value of the infinite domain solution $w^{\varepsilon,\eta}$ on the boundary of the micro box. Standard numerical homogenization recipes assume that the boundary condition for the local micro problem is restricted by the global macro data. However, as depicted in Figure 1, on the boundary of the local problem, the macro solution is $O(\varepsilon)$ away from $w^{\varepsilon,\infty}$. This mismatch on the boundary propagates into the interior of the domain and degrades the overall convergence rate.

2.2. Averaging error

For the averaging error we first prove an averaging lemma.

Lemma 1. *Let f be a 1-periodic bounded function such that $f \in L^\infty([0,1])$ and let $K \in \mathbb{K}^{p,q}$. Then, with $\bar{f} = \int_0^1 f(z)dz$ and $\varepsilon \le \eta$, we have*

$$\left| \int_{-\eta/2}^{\eta/2} K_\eta(t) f(t/\varepsilon) dt - \bar{f} \right| \le C|f|_\infty \left(\frac{\varepsilon}{\eta}\right)^{q+2}. \tag{18}$$

Moreover, assume that $f(t,s)$ is 1-periodic in s, and that $\partial_t^k f \in C([-\eta/2, \eta/2]; L^\infty([0,1]))$ for $k = 0, \dots, r$. Then, we have, with $\bar{f}(t) = \int_0^1 f(t,z)dz$ and $\varepsilon \le \eta \le 1$,

$$\left| \int_{-\eta/2}^{\eta/2} K_\eta(t) f(t, t/\varepsilon) dt - \bar{f}(0) \right| \le CC_f \begin{cases} \left(\frac{\varepsilon}{\eta}\right)^{q+2} + \eta^r & p \ge r \\ \left(\frac{\varepsilon}{\eta}\right)^{q+2} + \eta^{p+1} & p < r. \end{cases} \tag{19}$$

where the constant C does not depend on ε, η, f or s but may depend on K, p, q, r.

Proof. The estimate (18) is proved in [23] with a continuous f since all the derivatives were treated in classical sense. The same proof applies to $f \in L^\infty$ if the derivatives are seen in the weak sense, see Figure 2. To prove (19), set $\alpha = \dfrac{\varepsilon}{\eta}$, then

$$\int_{\mathbb{R}} K_\eta(t) f(t, t/\varepsilon) dt = \int_{-\eta/2}^{\eta/2} K_\eta(t) f(t, t/\varepsilon) dt = \int_{-1/2}^{1/2} K(t) f(\eta t, t/\alpha) dt$$
$$= \int_{-1/2}^{1/2} K(t) f(0, t/\alpha) dt + \sum_{j=1}^{r-1} \frac{\eta^j}{j!} \int_{-1/2}^{1/2} K(t) t^j \partial_t^j f(0, t/\alpha) dt + \frac{\eta^r}{r!} \int_{-1/2}^{1/2} K(t) t^r \partial_t^r f(\zeta_t, t/\alpha) dt$$
$$= I + II + III.$$

For the term I we use (18) and get

$$\left| I - \bar{f}(0) \right| \le C \left| f \right|_\infty \alpha^{q+2}.$$

To bound the term II, first we note that by Lemma 2.3 in [23]

$$\eta^j \int_{-1/2}^{1/2} K(t) t^j \partial_t^j f(0, t/\alpha) dt = \int_{-\eta/2}^{\eta/2} K_\eta(t) t^j \partial_t^j f(0, t/\varepsilon) dt \le CC_f \begin{cases} \alpha^{q+2}\eta^j & 1 \le j \le p \\ \alpha^{q+2}\eta^j + \eta^j & j > p. \end{cases}$$

Since $\eta < 1$, this will give then that

$$|II| \leq CC_f \begin{cases} \alpha^{q+2} & p \geq r, \\ \alpha^{q+2} + \eta^{p+1} & p < r. \end{cases}$$

Finally, for the last term we have

$$|III| = \frac{\eta^r}{r!} \left| \int_{-1/2}^{1/2} K(t) t^r \partial_t^r f(\zeta_t, t/\alpha) dt \right| \leq C_r C_f \eta^r.$$

□

By (14) we have

$$\int_{\Omega_\eta} K_\eta(\boldsymbol{x}) A(\boldsymbol{x}/\varepsilon) \nabla w^{\varepsilon,\eta}(\boldsymbol{x}) \, d\boldsymbol{x} = \int_{\Omega_\eta} K_\eta(\boldsymbol{x}) \left(A(\boldsymbol{x}/\varepsilon) + A(\boldsymbol{x}/\varepsilon) D_{\boldsymbol{y}} \boldsymbol{\chi}(\boldsymbol{x}/\varepsilon) \right) \, d\boldsymbol{x} \nabla \hat{u},$$

where $(D_{\boldsymbol{y}} \boldsymbol{\chi})_{i,j} = \partial_{y_i} \boldsymbol{\chi}_j$, and since $A(\boldsymbol{y}) + A(\boldsymbol{y}) D\boldsymbol{\chi}(\boldsymbol{y})$ for all $\boldsymbol{y} \in Y$ is 1-periodic in all directions we can apply Lemma 1 and use the relation (4) to conclude that

$$\begin{aligned} &\left| \int_{\Omega_\eta} K_\eta(\boldsymbol{x}) A(\boldsymbol{x}/\varepsilon) \nabla w^{\varepsilon,\infty}(\boldsymbol{x}) \, d\boldsymbol{x} - A^0 \nabla \hat{u} \right| \\ = &\left| \left(\int_{\Omega_\eta} K_\eta(\boldsymbol{x}) A(\boldsymbol{x}/\varepsilon) \left(I + D_{\boldsymbol{y}} \boldsymbol{\chi}(\boldsymbol{x}/\varepsilon) \right) \, d\boldsymbol{x} - \int_Y A(\boldsymbol{y}) \left(I + D_{\boldsymbol{y}} \boldsymbol{\chi}(\boldsymbol{y}) \right) \, d\boldsymbol{y} \right) \nabla \hat{u} \right| \\ &\leq C \left(\frac{\varepsilon}{\eta} \right)^{q+2} |\nabla \hat{u}|_\infty . \end{aligned}$$

This analysis shows that the averaging error can be made arbitrarily small by using averaging operators with higher q.

Remark 3. *In Figure 2, we illustrate the sharp rate of convergence from Lemma 1 for a discontinuous periodic function depicted in the left.*

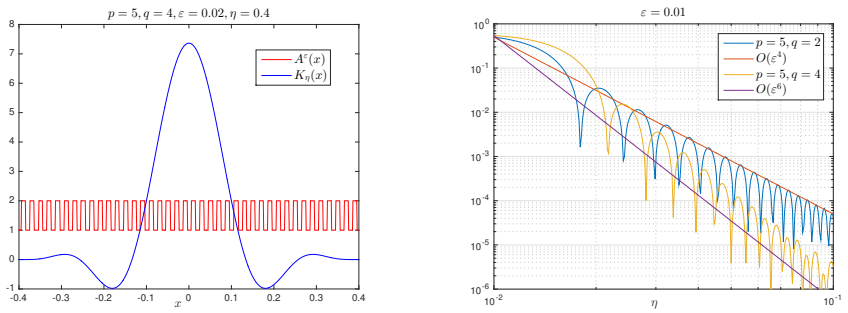

Figure 2: (Left) A $K \in \mathbb{K}^{5,4}$ is applied to an ε-periodic function A^ε. (Right) The sharp convergence rate, $O((\varepsilon/\eta)^{q+2})$, from Lemma 1 is observed by fixing $\varepsilon = 0.01$ and increasing η.

3. Micro problems with integral constraints

In the previous section, we saw that classical boundary conditions such as Dirichlet lead to a first order error $O(\varepsilon/\eta)$ in the flux approximation. In this section we study the possibility of enforcing nonclassical conditions to the PDE. In particular, we present a micro problem with an integral condition, which, in one dimension, captures the homogenized flux to arbitrarily high orders in ε/η. However, it leads to certain difficulties in higher dimensions, which we explain for the two dimensional case.

3.1. One dimension

The main idea of this one dimensional approach is to force the *average* of the derivative $\partial_x w^{\varepsilon,\eta}$ to equal to the derivative of the macroscopic state. For the micro domain $\Omega_\eta = [-\eta/2, \eta/2]$, the micro problem reads

$$\text{New Micro Problem:} \quad \begin{array}{l} -\partial_x \left(A^\varepsilon(x)\partial_x w^{\varepsilon,\eta}\right) = 0, \quad \text{in } \Omega_\eta \\ \int_{\Omega_\eta} K_\eta(x)\partial_x w^{\varepsilon,\eta}(x)\, dx = \partial_x \hat{u}(0), \end{array} \tag{20}$$

where $\hat{u} = sx$ is the given macroscopic state. To simplify the analysis, we assume that the media is locally periodic, i.e., $A^\varepsilon(x) = A(x, x/\varepsilon)$ and we will show that

$$F := \int_{\Omega_\eta} K_\eta(x) A^\varepsilon(x)\partial_x u^\varepsilon(x) dx = \hat{F} + O\left(\left(\frac{\varepsilon}{\eta}\right)^{q+2} + \eta^{p+1}\right),$$

where F is the HMM flux and $\hat{F}$ is the one-dimensional version of the homogenised flux defined in (10).

Remark 4. *We note here that the integral condition in* (20) *is not sufficient to guarantee uniqueness. Therefore, the micro problem* (20) *needs to be provided with another complementary condition. For example, one can set*

$$\int_{\Omega_\eta} K_\eta(x) w^{\varepsilon,\eta}(x) dx = 0. \tag{21}$$

With this additional requirement, one can easily show that the equation (20) *becomes a well-posed problem.*

Now to prove our claim we note from (20) that

$$A^\varepsilon(x)\partial_x w^{\varepsilon,\eta}(x) = C.$$

Then using the first integral condition in problem (20) and the Lemma 1 we obtain

$$\partial_x \hat{u} = \int_{\Omega_\eta} K_\eta(x)\partial_x w^{\varepsilon,\eta}(x)\, dx = C \int_{\Omega_\eta} K_\eta(x) \frac{1}{A^\varepsilon}\, dx = C\left(\frac{1}{A^0} + O\left(\left(\frac{\varepsilon}{\eta}\right)^{q+2} + \eta^{p+1}\right)\right).$$

Therefore $C = A^0\partial_x \hat{u} + O\left((\varepsilon/\eta)^{q+2} + \eta^{p+1}\right) = \hat{F} + O\left((\varepsilon/\eta)^{q+2} + \eta^{p+1}\right)$, and

$$F = \int_{\Omega_\eta} K_\eta(x) A^\varepsilon(x)\partial_x w^{\varepsilon,\eta}\, dx = C = \hat{F} + O\left(\left(\frac{\varepsilon}{\eta}\right)^{q+2} + \eta^{p+1}\right).$$

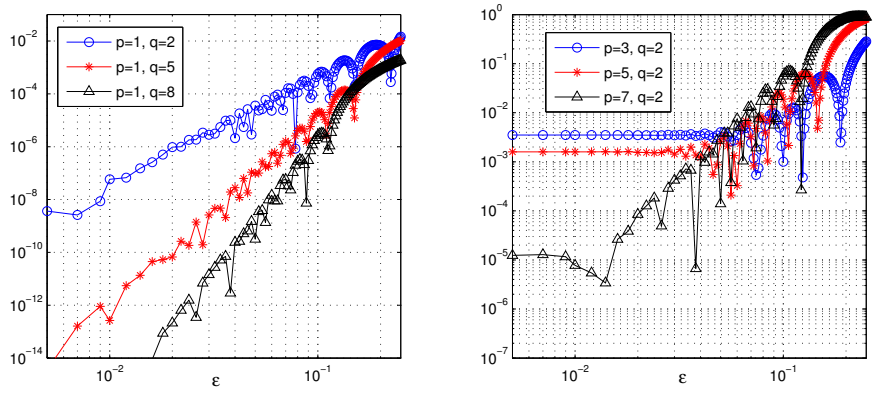

Figure 3: Error between HMM flux and the homogenized flux for periodic (left) and non-periodic (right) media. The one dimensional problem (20) is solved over a box of size $\eta = 0.25$. The periodic and locally-periodic coefficients are chosen to be $A^\varepsilon(x) = e^{\cos(2\pi x/\varepsilon + 0.2)}$, and $A^\varepsilon(x) = 1.1 + sin(2\pi x) + e^{\cos(2\pi x/\varepsilon+0.2)}$ respectively.

By Lemma 1, in purely-periodic media the term η^{p+1} in the error vanishes. Hence

$$\left|F - \hat{F}\right| \leq \begin{cases} O\left(\left(\frac{\varepsilon}{\eta}\right)^{q+2}\right) & \text{if } A \text{ is periodic,} \\ O\left(\left(\frac{\varepsilon}{\eta}\right)^{q+2} + \eta^{p+1}\right) & \text{if } A \text{ is locally-periodic.} \end{cases} \tag{22}$$

This shows that one can obtain arbitrarily high order of convergence upon using the integral condition in (20) , and that, at least in one dimension, one does not need to use a filter in the definition of the micro problem as was the case in [15], cf. (11). The numerical results in Figure 3 agrees well with the expected convergence rates in (22).

3.2. Generalization to higher dimensions

A natural way to extend the previous idea to higher dimensions is to impose the condition

$$\int_{\Omega_\eta} K_\eta(x_1) K_\eta(x_2) \nabla w^{\varepsilon,\eta}(x_1, x_2) dx = \nabla \hat{u}(0,0) \tag{23}$$

to the PDE

$$-\nabla \cdot (A^\varepsilon(\boldsymbol{x}) \nabla w^{\varepsilon,\eta}(\boldsymbol{x})) = 0, \quad \text{in } \Omega_\eta. \tag{24}$$

However, the condition (23) is not sufficient for the well-posedness of the micro problem even if we add the condition (21). The system becomes underdetermined unless we impose additional conditions to the PDE (24). In [15], the authors picked the solution leading to minimum energy, cf. (11). Through this strategy, they were able to obtain $O((\varepsilon/\eta)^2)$ convergence rates for periodic problems. Here we want to think of other ways of generalizing the one dimensional approach above. We discuss two potential ways of

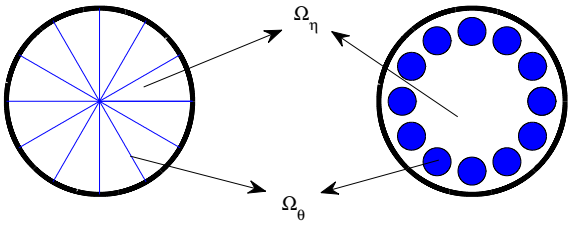

Figure 4: Two microscopic domains, where Ω_η represents the micro domains, and Ω_θ indicates the region where the integral condition is imposed. Left: Radial averaging. The micro solution is averaged over each radius in the circle. Right: Circular averaging. The solution is averaged over small circles near the boundary.

imposing integral conditions. The first idea is the circular averaging shown in the right plot of Figure 4, where we restrict the averages of the solution over some circles in each radial direction to equal to the homogenized solution. The second approach is the radial averaging, depicted in the left plot of Figure 4, where the average of the solution in each radial direction is forced to equal to the homogenized solution. For both of the approaches we face the following important questions: (1) Will the PDE together with the integral conditions lead to a well-posed system or not? (2) Will the flux of the micro problem average to the homogenized flux as $\varepsilon \to 0$? Through some simplifying assumptions we will motivate that the first averaging approach (averaging over balls in a circular domain) suffers from a well-posedness problem and the second approach (averaging over curves), though well-posed, suffer from a convergence problem.

3.2.1. Circular averaging

Without loss of generality we assume that the micro box $\Omega_\eta \subset \mathbb{R}^2$ is a ball of radius $r_0+\eta$ centered at the origin, i.e., $\Omega_\eta = B(0, r_0+\eta)$, where $r_0 > \eta$. We consider again the linear macroscopic state $\hat{u}(\boldsymbol{x}) = \mathbf{s}\cdot\boldsymbol{x}$. Let $\hat{s}(\theta) = (\cos(\theta), \sin(\theta))$. We force the averages of the microscopic solution $w^{\varepsilon,\eta}$ to equal to $\hat{u}$ over smalls balls Ω_θ centered at $r_0\hat{s}(\theta)$, and defined as $\Omega_\theta := B(r_0\hat{s}(\theta), \eta) = \{\boldsymbol{x} \in \mathbb{R}^2 |\quad |\boldsymbol{x} - r_0\hat{s}(\theta)| \le \eta\}$, as depicted in Figure 4. Then the microscopic problem reads

$$\text{Micro Problem (circular):} \quad \begin{array}{l} -\nabla\cdot(A^\varepsilon \nabla w^{\varepsilon,\eta}_{circ}(\boldsymbol{x})) = 0, \quad \text{in } \Omega_\eta := B(0, r_0+\eta), \\ \int_{\Omega_\theta} \tilde{K}_{|\Omega_\theta|}(\boldsymbol{x} - r_0\hat{s}(\theta)) w^{\varepsilon,\eta}_{circ}(\boldsymbol{x})\, d\boldsymbol{x} = \hat{u}(r_0\hat{s}(\theta)), \quad 0 \le \theta \le 2\pi, \end{array} \tag{25}$$

where $\tilde{K}$ is a mollifier, compactly supported in the unit ball, ex. $\tilde{K}(\boldsymbol{x}) = e^{-1/(1-|\boldsymbol{x}|^2)}$. To study the well-posedness of the above problem we look at the simpler constant coefficient problem and consider only constant averaging kernels. The simplifid equation is:

$$\begin{array}{l} \Delta w = 0, \quad \text{in} \quad |\boldsymbol{x}| \le r_0 + \eta, \\ \frac{1}{|\Omega_\theta|}\int_{\Omega_\theta} w\, d\boldsymbol{x} = \hat{u}(r_0\hat{s}(\theta)). \end{array} \tag{26}$$

Since u is harmonic, the mean value formula for harmonic functions tells us that

$$u(r_0\hat{s}(\theta)) = \frac{1}{|\Omega_\theta|}\int_{\Omega_\theta} w\, d\boldsymbol{x} = \hat{u}(r_0\hat{s}(\theta)).$$

In the interior $B(0, r_0)$, the solution w will, thus, solve a simple Laplace equation with smooth Dirichlet boundary conditions $\hat{u}(\boldsymbol{x}) = \mathbf{s}\cdot\boldsymbol{x}$. The existence and uniqueness of w follows from the integral representation of the solution and the maximum principle for elliptic PDEs respectively. Furthermore, the stability of the solution follows by standard estimates for elliptic PDEs

$$\| w \|_{H^1(B(0,r_0))} \leq C_{B(0,r_0)} \| \hat{u} \|_{H^1(B(0,r_0))} . \tag{27}$$

Therefore the solution w is well-posed in the interior of the domain $B(0, r_0)$. However, note that in (26) the averaging takes place in the ball Ω_θ which uses the solution also outside $B(0, r_0)$; more precisely, inside the boundary layer $B(0, r_0 + \eta) \setminus B(0, r_0)$. In this respect, it is important to know the behavior of the solution in this boundary layer. To answer this question we consider the Laplace operator in polar coordinates and write

$$r^2\partial_{rr}w + r\partial_r w + \partial_{\theta\theta}w = 0.$$

Now if

$$\hat{u}\left(r_0\hat{s}\left(\theta\right)\right) = \sum_{k=0}^{\infty} \hat{g}_k e^{ik\theta},$$

then by separation of variables we have

$$w(r,\theta) = \sum_{k=0}^{\infty} \hat{g}_k \left(\frac{r}{r_0}\right)^k e^{ik\theta}.$$

This shows that the response to a small perturbation in the data $\hat{u} = \varepsilon e^{ik\theta}$ will be

$$w(r,\theta) = \left(\frac{r}{r_0}\right)^k \varepsilon e^{ik\theta}.$$

Hence for $r > r_0$, i.e., outside the domain $B(0, r_0)$, the solution blows up as $k \longrightarrow \infty$.

Since the flux is only computed using the solution in the interior, the procedure still works for the constant coefficient case. However, the situation with the oscillatory problem (25) is trickier. In this case, the solution $w^{\varepsilon,\eta}_{circ}$ is not harmonic and therefore the mean value formula does not hold. Hence, the growth of the solution in the boundary layer might propagate into the interior domain. What is relevant for us is to check if this propagation influences the convergence as $\varepsilon \longrightarrow 0$ of $w^{\varepsilon,\eta}_{circ}$ to $\hat{u}$ in the interior of $B(0, r_0)$. Figure 5 illustrates the difference between the oscillatory solution and the homogenized solution over discs with different radii. In this simulation we pose the micro problem (25) over the unit circle. We fix the support $\eta = 0.2$ of the averaging kernel so that $r_0 = 0.8$, and look at the max norm error between $w^{\varepsilon,\eta}_{circ}$ and $\hat{u}$ for different ε. The results clearly show that all the points in $B(0, 1)$ are influenced by the blow up close to the boundary. Therefore, there is no $r < r_0$ such that

$$w^{\varepsilon,\eta}_{circ}(\boldsymbol{x}) \longrightarrow \hat{u}(\boldsymbol{x}) \text{ as } \varepsilon \longrightarrow 0, \quad \boldsymbol{x} \in B(0, r).$$

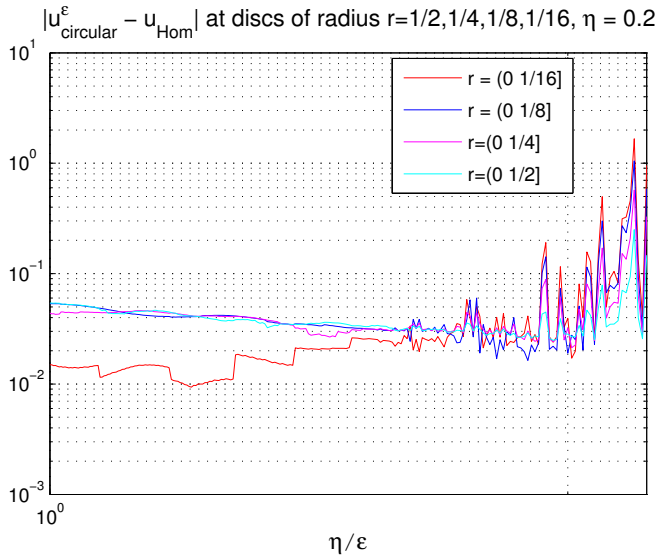

Figure 5: The maximum norm difference beween $w^{\varepsilon,\eta}_{circ}(x)$ and the homogenized solution $\hat{u} = x+y$ inside discs of different radii $r = 1/2, 1/4, 1/8, 1/16$ is shown. This plot shows that there is no convergence (as $\varepsilon \longrightarrow 0$) of $w^{\varepsilon,\eta}_{circ}(x)$ to $\hat{u}$ even in the interior of the domain. The error becomes more pronounced as we take smaller ε. In this simulation we have used 30 points per ε.

3.2.2. Radial averaging

The main idea behind radial averaging is to equate the average of the microscopic solution in the radial directions with the macroscopic data. We define the domain $\Omega_\eta = B(0,\eta) \subset \mathbb{R}^2$ and we again assume linear macroscopic data $\hat{u}(\boldsymbol{x}) = \mathbf{s}\cdot\boldsymbol{x}$, and introduce the micro problem:

$$\text{Micro Problem (Radial):} \quad \begin{array}{l} -\nabla\cdot(A^\varepsilon \nabla w^{\varepsilon,\eta}_{radial}(\boldsymbol{x}))= 0, \quad \text{in} \quad \Omega_\eta \\ \int_0^\eta K_\eta(\zeta - \frac{\eta}{2}) w^{\varepsilon,\eta}_{radial}(\zeta\hat{s}(\theta))\, d\zeta = \hat{u}(\frac{\eta}{2}\hat{s}(\theta)), \end{array} \tag{28}$$

To study the well-posedness of this problem, we consider the constant coefficient problem as above,

$$-\Delta w = 0.$$

Furthermore, to simplify the analysis we assume that $\eta = 1$ and $K = 1$ in $[-1/2, 1/2]$. The integral condition in (28) is then

$$\int_0^1 w(\zeta\hat{s}(\theta))d\zeta = g(\theta), \qquad \text{where } g(\theta) = \hat{u}\left(\frac{1}{2}\hat{s}\,(\theta)\right).$$

Since the solution w is a harmonic function, it can be expressed as the real part of a complex analytic function J such that $J(x_1 + ix_2) = w(x_1, x_2) + iv(x_1, x_2)$. We express J in terms of a power series

$$J(z) = \sum_{k=0}^{\infty} \hat{J}_k z^k.$$

Then, with $z_1(\theta) = \cos(\theta) + i\sin(\theta)$, we have

$$g(\theta) = \Re \int_0^1 J(sz_1(\theta))ds = \Re \sum_{k=0}^{\infty} \hat{J}_k \int_0^1 (sz_1(\theta))^k ds = \Re \sum_{k=0}^{\infty} \frac{\hat{J}_k}{k+1} z_1(\theta)^k.$$

Now let $G(z)$ be the analytic function defined by the Taylor's coefficients $\hat{G}_k = \hat{J}_k/(k+1)$. This implies that $J = \partial_z(zG)$ and therefore, J can be identified uniquely through G. Then we can rewrite the last equation as

$$g(\theta) = \Re G(z_1(\theta)) = \Re G(e^{i\theta}). \tag{29}$$

Now using $G(x_1 + ix_2) = h(x_1, x_2) + iu(x_1, x_2)$ we get

$$\hat{u}\left(\frac{\hat{s}(\theta)}{2}\right) := g(\theta) = h(\hat{s}(\theta)).$$

On the other hand, since $h(x_1, x_2)$ is harmonic it satisfies the Laplace equation with boundary data given by $\hat{u}$

$$\begin{array}{cc} -\Delta h = 0, & \text{in} \quad \Omega \\ h(\hat{s}(\theta)) = \hat{u}(\theta) & \text{on } |\boldsymbol{x}| = 1. \end{array}$$

The well-posedness of the above problem is a classical matter, and the solution h enjoys the same stability estimate as before in (27). The above problem is well-posed and therefore has a unique solution h. Finally, using Cauchy Rieman equations $\partial_{x_1} h = \partial_{x_2} u, \partial_{x_2} h = -\partial_{x_1} u$, we can express w in terms of h as follows

$$\begin{aligned} w &= \Re J = \Re \partial_z \left(zG(z)\right) = \Re G + \Re \left(z \partial_z G(z)\right) \\ &= h + \Re \left((x_1 + ix_2) \left(\frac{1}{2} \left(\partial_{x_1} h + \partial_{x_2} u \right) + \frac{i}{2} \left(\partial_{x_2} h - \partial_{x_1} u \right) \right) \right) \\ &= h + x_1 \partial_{x_1} h + x_2 \partial_{x_2} h. \end{aligned}$$

The well-posedness of w follows readily from that of h. However, we note that an H^1 regularity for h implies an L^2 regularity for w. This is mainly due to the integral condition in (28) which requires less regularity for the solution.

Now let us consider the oscillatory micro-problem (28). By the previous analysis, we have good enough evidence for the well-posedness of the above problem for a fixed ε. However, remember that our eventual concern is if the HMM flux $\boldsymbol{F} = \left(\mathcal{K} A^\varepsilon \nabla w^{\varepsilon,\eta}_{radial}\right)(0)$ converges to the homogenized flux $\hat{\boldsymbol{F}} = A^0 \nabla \hat{u}$, as $\varepsilon \to 0$? To have an idea about this, we perform a numerical simulation with $\eta = 1$, and $K \in \mathbb{K}^{1,2}$, and we plot the difference between the homogenized flux and the HMM fluxes as we refine the small parameter ε. Figure 6 depicts the error between the HMM flux and the homogenized flux for varying ε. This result does not show convergence, as $\varepsilon \to 0$, for the HMM flux.

To explain this failure we resort to [24] in which the authors proved that, in general, integrals of locally-periodic functions over surfaces Γ in $\mathbb{R}^d$ may not have a unique limit. Indeed, they found that the unique limit depends on the orientation of the normal vectors on the surface. To be more precise, let Γ be a C^1 surface in $\mathbb{R}^d$ which is not necessarily

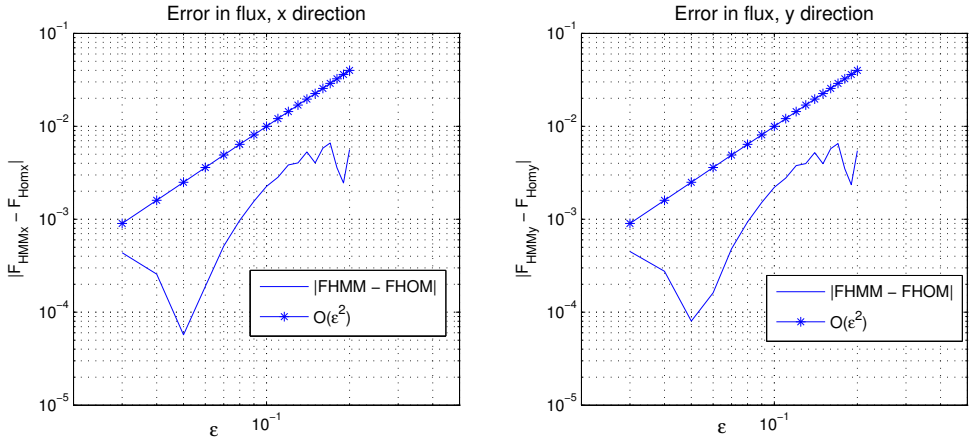

Figure 6: Difference between the HMM and homogenized fluxes in both spatial directions is shown. A kernel from $\mathbb{K}^{1,2}$ is used in this simulation. Rest of the data are the same as in Figure 7.

bounded, and $f^\varepsilon(\boldsymbol{x}) = f(\boldsymbol{x}, \boldsymbol{x}/\varepsilon)$ where $f(\boldsymbol{x}, \boldsymbol{y})$ is Y-periodic in $\boldsymbol{y}$, and let $f(\boldsymbol{x}, \boldsymbol{y})$ be integrable in the $\boldsymbol{x}$-variable over Γ. Then, in general, the integral

$$I_\Gamma[f^\varepsilon] = \int_\Gamma f^\varepsilon(\boldsymbol{x})\, d\sigma_{\boldsymbol{x}}$$

does not have a unique limit as $\varepsilon \to 0$. Here $\sigma_{\boldsymbol{x}}$ stands for the surface measure. The unique limit exists if the surface Γ has an irrational normal almost everywhere on Γ, where irrationality of a vector is defined as:

Definition 1. *Let* $\mathbf{n}$ *be a vector in* $\mathbb{R}^d$*, then*

- $\mathbf{n}$ *is rational direction if there exists a real number* α *such that* $\alpha\mathbf{n} \in \mathbb{Z}^d$.
- $\mathbf{n}$ *is irrational direction if it is not rational.*

This explains the link between our flux convergence failure and the theory of integrals of oscillatory functions. In our setting, we are forcing the averages of the solution along every radius. Remember that we want the micro solution to be as close to the infinite solution $w^{\varepsilon,\infty}$ as possible. For this reason, suppose that $w^{\varepsilon,\eta}_{radial}$ is very close to $w^{\varepsilon,\infty}$ such that we average $w^{\varepsilon,\infty}$ (instead of $w^{\varepsilon,\eta}_{radial}$) in radial directions. Since the averaging takes place for every $0 \leq \theta \leq 2\pi$, there will always be a rational direction θ^* such that

$$\lim_{\varepsilon \longrightarrow 0} \int_0^\eta w^{\varepsilon,\infty}(\zeta \hat{s}(\theta^*)) d\zeta \neq \hat{u}\left(\frac{\eta}{2}\hat{s}(\theta^*)\right).$$

This implies that $w^{\varepsilon,\eta}_{radial}$ should deviate from $w^{\varepsilon,\infty}$ due to the integral condition

$$\int_0^\eta w^{\varepsilon,\eta}_{radial}(\zeta \hat{s}(\theta^*)) d\zeta = \hat{u}\left(\frac{\eta}{2}\hat{s}(\theta^*)\right).$$

Another problem is related to the convergence rate. In principle, for almost all the directions we do have convergence. However, the convergence rate will be very slow in

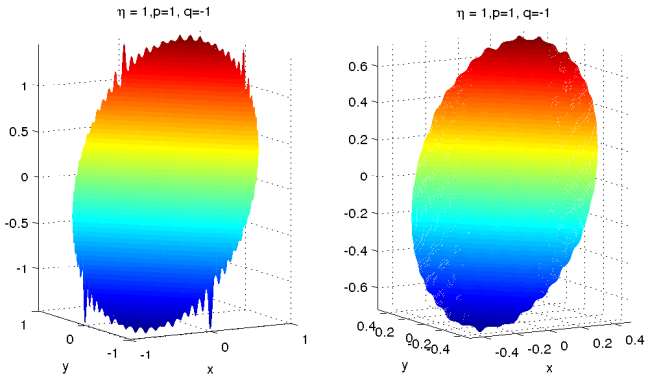

Figure 7: The oscillatory problem (20) , with $A^\varepsilon(x) = (1.5 + \sin(2\pi x_1/\varepsilon))(1.5 + \sin(2\pi x_2/\varepsilon))$, $\varepsilon = 0.08$, $\eta = 1$, $K \in \mathbb{K}^{1,-1}$ and data $\hat{u}(\boldsymbol{x}) = x_1 + x_2$, is solved over the unit circle. The plot on the left shows the solutions over the unit circle $B(0,1)$, and the plot on the right shows the solution in $B(0, \frac{1}{2})$.

certain directions. This is due to the fact that certain directions will be close to rational directions and then see far less oscillations than the rest of the directions.

To test our theoretical arguments we perform a numerical simulation showing the solution of the micro problem. In Figure 7 we use $\eta = 1$, and a constant kernel with $(p, q) = (1, -1)$, and we give a plot of the solution over the entire domain $\Omega = B(0, 1)$ and the interior domain $B(0, \frac{1}{2})$. As we see in the left plot, the solution at certain directions tends to have an $O(1)$ deviation from the average. On the other hand, we do not see this $O(1)$ deviation in the interior $B(0, \frac{1}{2})$. This good behavior in the interior does not seem to save the convergence of the flux as already depicted in Figure 6. Hence, restricting the oscillatory solution over surfaces in $\mathbb{R}^d$ does not seem to be a good idea to capture homogenized parameters.

4. A time dependent approach

The main idea in this paper is to use a time-dependent hyperbolic PDE as our micro-model. Because of the finite speed of propagation, the boundary conditions will then not affect the solution in the interior sufficiently far from the boundary. We pose a second-order multi-scale wave equation on $I_\tau \times \Omega_{\eta,\boldsymbol{x}_0}$, where $I_\tau := [0, \tau/2]$ and $\tau/2$ is the final time for the micro simulations, and $\Omega_{\eta,\boldsymbol{x}_0} = [-L_\eta + \boldsymbol{x}_0, L_\eta + \boldsymbol{x}_0]^d$ is the spatial domain. We assume that $L_\eta = \frac{\eta}{2} + \frac{\tau}{2}\sqrt{|A^\varepsilon|_\infty}$ such that the boundary data does not affect the solution in the region $I_\tau \times [-\eta/2, \eta/2]^d$. Moreover, as in the previous sections we assume a linear macroscopic data denoted by $\hat{u} = \mathbf{s} \cdot \boldsymbol{x}$. The micro problem (8) is then modified to

$$\text{New Micro Problem:} \quad \begin{array}{c} \partial_{tt} w^{\varepsilon,\eta}(t,\boldsymbol{x}) - \nabla \cdot (A^\varepsilon(\boldsymbol{x}) \nabla w^{\varepsilon,\eta}(t,\boldsymbol{x})) = 0 \quad \text{in} \quad I_\tau \times \Omega_{\eta,\boldsymbol{x}_0}, \\ w^{\varepsilon,\eta}(0,\boldsymbol{x}) = \hat{u}(\boldsymbol{x}) \quad \partial_t w^{\varepsilon,\eta}(0,\boldsymbol{x}) = 0, \end{array} \tag{30}$$

The equation is equipped with periodic boundary conditions, i.e., $w^{\varepsilon,\eta} - \hat{u}$ is periodic on the cell $\Omega_{\eta,\boldsymbol{x}_0}$. We define the averaging operator in time and space as follows:

$$\left(\mathcal{K}_{\tau,\eta} * f\right)(t,\boldsymbol{x}) := \int_{-\frac{\tau}{2}+t}^{\frac{\tau}{2}+t} \int_{\Omega_{\eta,\boldsymbol{x}}} K_\tau(\tilde{t}-t) K_\eta(\tilde{\boldsymbol{x}}-\boldsymbol{x}) f(\tilde{t},\tilde{\boldsymbol{x}}) d\tilde{\boldsymbol{x}}\, d\tilde{t}. \tag{31}$$

Then HMM computes the flux by

$$\text{Upscaling: } \boldsymbol{F}(\boldsymbol{x}_0) = \left(\mathcal{K}_{\tau,\eta} * A^\varepsilon \nabla w^{\varepsilon,\eta}\right)(0,\boldsymbol{x}_0). \tag{32}$$

The goal is that the HMM flux $\boldsymbol{F}(\boldsymbol{x}_0)$ should approximate the homogenized flux

$$\hat{\boldsymbol{F}}(\boldsymbol{x}_0) = A^0(\boldsymbol{x}_0)\nabla\hat{u} = A^0(\boldsymbol{x}_0)\nabla\hat{u}. \tag{33}$$

Note that the upscaling step (32) requires information about the gradient $\nabla w^{\varepsilon,\eta}$ for $t < 0$. However, since $\partial_t w^{\varepsilon,\eta}(0,\boldsymbol{x}) = 0$ we have the symmetry $w^{\varepsilon,\eta}(t,\boldsymbol{x}) = w^{\varepsilon,\eta}(-t,\boldsymbol{x})$.

Remark 5. *In the method, we always assume that $\tau = \eta$. In practice, the choice $\tau = \eta = O(\varepsilon)$ gives qualitatively satisfactory macroscopic solutions and the theory is not restricted by this assumption.*

The intuition behind this strategy is based on the following facts:

- In [25], the micro model (30) is naturally used to approximate the coefficient of the homogenized wave equation

$$\partial_{tt} u^0(t,\boldsymbol{x}) - \nabla\cdot\left(\hat{A}\nabla u^0(t,\boldsymbol{x})\right) = f(\boldsymbol{x}), \quad t\in[0,T], \tag{34}$$

  However, for short time scales $T = O(1)$, the effective wave equation (34) possesses the same homogenized coefficient $\hat{A}$ as that of homogenized elliptic problem (3), see e.g. [1, 3].

- The solutions of hyperbolic PDEs propagate with finite speed. Thus, the error due to the boundary will not affect the interior solution if the microscopic domain is large enough.

- In the periodic setting, the time average of the wave equation (30) matches the infinite domain solution $w^{\varepsilon,\infty}$ defined in Section 2.

It should be noted that higher accuracy is achieved by choosing smoother kernels with more vanishing moments. In purely periodic media, the following theorem was proved, in [25], for multiscale wave propagation.

Theorem 2. *(Theorem 3.1 in [25]) Let $\hat{\boldsymbol{F}}(\boldsymbol{x}_0)$ be given by (33), and $\boldsymbol{F}(\boldsymbol{x}_0)$ be defined by (32) with $K \in \mathbb{K}^{p,q}$ where $w^{\varepsilon,\eta}(t,\boldsymbol{x})$ solves the micro problem (30) with the initial data $\hat{u} = \mathbf{s}\cdot\boldsymbol{x}$ exactly, and suppose $A^\varepsilon(\boldsymbol{x}) = A(\boldsymbol{x}/\varepsilon)$, where $A \in (C^\infty(Y))^{d\times d}$ is a Y-periodic matrix function satisfying (2), and $\tau = \eta$ with $\varepsilon \le \eta \le 1$. Then*

$$\left|\boldsymbol{F}(\boldsymbol{x}_0) - \hat{\boldsymbol{F}}(\boldsymbol{x}_0)\right| \le C\left(\frac{\varepsilon}{\eta}\right)^{q+2} |\mathbf{s}|_\infty,$$

where $|\mathbf{s}|_\infty := \max_{1\le j\le d}|s_j|$, and C is a constant independent of ε and η.

Remark 6. *The proof of the Theorem 2 is based on an L^2 eigenfunction expansion of the local solution, see [25] Theorem* 3.1. *The smoothness requirement in Theorem 2 is only to simplify the analysis and the same result will be true also for less regular A. See Figure 8 where an example of a discontinuous layered media is given. The coefficient A^ε does not satisfy the smoothness assumption of Theorem 2 but the method still enjoys the precise $O((\varepsilon/\eta)^{q+2})$ convergence rate for a kernel $K \in \mathbb{K}^{p,q}$ with $p = 5$ and $q = 4$.*

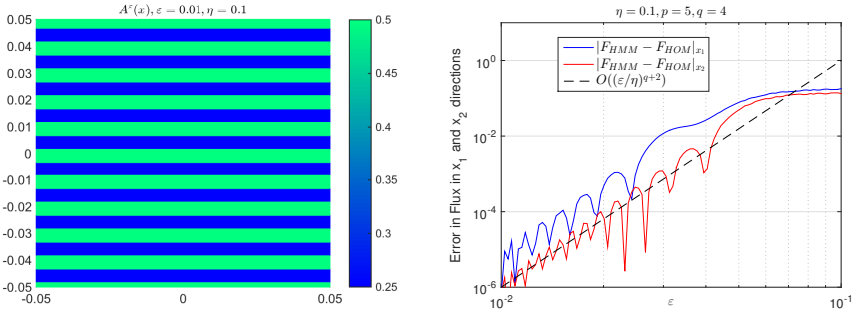

Figure 8: (Left) An ε-periodic discontinuous layered media, with $\varepsilon = 0.01$, on a two-dimensional domain Ω_η with $\eta = 0.1$ is depicted. (Right) The sharp convergence rate, $O((\varepsilon/\eta)^{q+2})$, from Theorem 2 is observed by fixing $\tau = \eta = 0.1$ and decreasing ε. In this simulation, the micro problem (30) is solved with the initial data $\hat{u} = \mathbf{s} \cdot \boldsymbol{x}$ where $\mathbf{s} = (1, 1)$. The HMM flux $\boldsymbol{F}$ is compared to the exact homogenised flux $\hat{\boldsymbol{F}} = A^0 \nabla \hat{u}$, where $A^0 = diag(1/3, 3/8)$, and hence $\hat{\boldsymbol{F}} = (1/3, 3/8)$.

Although the above theorem was proved in the context of multi-scale wave propagation where the original multi-scale PDE was a second-order wave equation, we can use the same theorem in the setting of multi-scale elliptic problems due to the fact that effective equations for both problems have excatly the same homogenized coefficient A^0, [1, 3]. This, in turn, implies that our time-dependent approach performs optimally in the periodic setting. By optimality we mean that the decay rate of the error $O((\varepsilon/\eta)^{q+2})$ in the HMM approximation can be made as small as we like by choosing high enough q.

In locally-periodic media, the situation is slightly different. For locally-periodic coefficients, preliminary theoretical results and numerical evidence in [26, 27] suggest an error of the type

$$E_{HMM} = O(\varepsilon + (\varepsilon/\eta)^{q+2})$$

for a kernel $K \in \mathbb{K}^{p,q}$ with $p > 1$ and $\tau = \eta \approx \varepsilon^{1-\beta}$, for $0 \leq \beta \leq 1/7$. It is worth mentioning that a certain degree of regularity such as $\partial_x^k A \in C(\overline{\Omega}; L^\infty(Y))$, at least for $k \leq 2$, is needed for this result to be true. Moreover, the error will be optimised for the following choice for the parameters η, τ, p, q:

1. $\tau = \eta = O(\varepsilon^{1-\beta})$, with $0 \leq \beta \leq 1/7$
2. $p > 1$
3. $q = \frac{1}{\beta} - 2$,

which will then yield $E_{HMM} \leq C_{p,q}\varepsilon$.

Note that the computational cost of solving the micro problem decreases with decreasing β. Moreover, arbitrarily small values for β are obtained by using kernels $K \in \mathbb{K}^{p,q}$ with better regularity properties, i.e., large q. Note that q can be chosen arbitrarily high with no influence on the computational cost of solving the micro problem (30).

Remark 7. *If $p = 1$, then we get an additional $O(\eta^{p+1})$ error in the locally-periodic media. This error is due to the local averaging of the slow variations in the media and can be removed if $p > 1$, see Figure 10.*

4.1. Computational cost in the periodic setting

As in the case of elliptic micro problems, the computational cost of solving the micro problem (30) is still independent of the small scale parameter ε since the computational box (in time and space) is in practice of size $O(\varepsilon)$. In Table 1, we compare the computational cost for reaching a fixed tolerance TOL of the wave equation to the cost of solving an elliptic problem as the micro problem. Note that in this comparison table, we assume that the cost of solving a linear system is proportional to the number of degrees of freedom which is valid, for example, if one uses multigrid solvers. In the periodic setting, if we use the wave equation as the micro problem we have $O((\varepsilon/\eta)^{q+2})$ error for an arbitrarily large q . On the other hand, if we use an elliptic equation as in (12) we can obtain $O((\varepsilon/\eta)^k)$ with $k = 4$ at best. Table 1 shows that for a fixed tolerance TOL, the computational cost of using the wave equation (30) is less than the computational cost of solving the elliptic PDE (12) if

$$1 + 1/d \leq (q + 2)/k.$$

Micro problem	Comp. cost	Error	Cost for a fixed tolerance TOL
Elliptic	$(\eta/\varepsilon)^d$	$(\varepsilon/\eta)^k$	$\mathrm{TOL}^{-d/k}$
Wave Equation	$(\eta/\varepsilon)^{d+1}$	$(\varepsilon/\eta)^{q+2}$	$\mathrm{TOL}^{-(d+1)/(q+2)}$

Table 1: Elliptic micro problem vs the wave equation approach

To make the comparison more fair, we must also emphasize that the zero-order reguralisation approach (12) has been analysed rigorously for periodic coefficients, for a subclass of almost periodic functions and also for the subclass of random coefficients which satisfy a spectral gap estimate, under a mild assumption of L^∞ for A^ε, see [17]. Moreover, from practical point of view it is much easier to solve (12) as it is a simple elliptic PDE. The mathematical analysis of the HMM described here, however, is available for C^∞ coefficients in periodic media but holds true also for less regular coefficients, see the proof of Theorem 3.1 in [25] and Remark 6. Moreover, the locally-periodic theory of the HMM is based on the findings in [26, 27] and will be reported later as an extension of the present work. What appears to be crucial from the locally-periodic analysis is that the HMM requires at least a certain degree of smoothness in the slow variable to give the desired rates.

5. Numerical results

In this section, we provide evidence that

- The time dependent approach gives $O((\varepsilon/\eta)^{q+2})$ convergence rate in the periodic setting, where q can be chosen arbitrarily large.
- If $p > 1$, we get $O(\varepsilon^k + (\frac{\varepsilon}{\eta})^{q+2})$ convergence rates in locally-periodic media, where $k = 2$ for $d = 1$ and $k = 1$ for $d \geq 2$. If $p = 1$, an additional $O(\eta^{p+1})$ error appears.
- For quasi-periodic problems, where the coefficient function oscillates with a rational and an irrational wavelength at the same time, the approach gives high order convergence rates similar to the periodic case.

First we will present results showing the convergence of the HMM flux to the homogenized flux. We then provide examples showing that the full HMM solution captures the homogenized solution. In all the examples, we will solve the micro problem (30) on the micro domain $I_\tau \times \Omega_{\eta,\boldsymbol{x}_0}$, where $I_\tau := (0, \tau/2]$ and $\Omega_{\eta,\boldsymbol{x}_0} = [-L_\eta + \boldsymbol{x}_0, L_\eta + \boldsymbol{x}_0]$. We always choose $\tau = \eta$ and $L_\eta = \frac{\eta}{2} + \frac{\tau}{2}\sqrt{|A^\varepsilon|_\infty}$. The values of ε and η will be specified in each example separately.

5.1. Convergence of flux in one dimension

The periodic case: We start with three periodic examples in one dimension. The periodic coefficients are given by

$$\begin{aligned} A_1^\varepsilon(x) &= 1.1 + \sin(2\pi x/\varepsilon), \quad A_2^\varepsilon(x) = e^{\cos(2\pi x/\varepsilon + 1)}, \\ A_3^\varepsilon(x) &= 1.1 + \sin(2\pi x/\varepsilon + 1)^2 + \frac{1}{2}\cos(2\pi x/\varepsilon + 1.1) \end{aligned} \tag{35}$$

The error in the flux for the simulations of the above periodic coefficients are given in Figure 9. In order to test the convergence rate we use a fixed micro cell-size $\eta = 0.01$, and we let $\varepsilon \longrightarrow 0$. For different p, q pairs, the simulations illustrate the $O((\varepsilon/\eta)^{q+2})$ convergence rate. All of the results agree with the statement of the Theorem 2. Note that, in these simulations, the homogenized coefficients are computed by a simple trapezoidal rule with an accuracy of 10^{-14}, and we have used the initial data $\hat{u} = x$.

The locally-periodic case: Here we consider the problem (30) with the following locally-periodic coefficient:

$$A^\varepsilon(x) = 1.1 + \frac{1}{2}\left(\sin(2\pi x + 0.1) + \sin(2\pi x/\varepsilon + 2)\right)$$

and show the convergence of flux. Figure 10 shows the $O(\varepsilon^2 + (\varepsilon/\eta)^{q+2})$ error in the flux approximation. Note that the constant error which appears when $p = 1$ is due to $O(\eta^{p+1})$ averaging error. As depicted in the figure, this error vanishes as we take $p > 1$.

5.2. Convergence of flux in two dimensions

The periodic case: We consider the problem (30) in two dimensions with the linear initial data $\hat{u} = x_1 + x_2$. The coefficient matrix is chosen to be

$$A^\varepsilon(\boldsymbol{x}) = (1.1 + \frac{1}{2}\sin(2\pi x_1/\varepsilon))(1.1 + \frac{1}{2}\sin(2\pi x_2/\varepsilon))I,$$

where I is (2×2) identity matrix. The homogenized coefficient and homogenized fluxes are explicitly given by

$$A^0 = \left(1.1\sqrt{1.1^2 - 0.25}\right) I, \quad \hat{\boldsymbol{F}} = (\hat{F}^1, \hat{F}^2), \quad \hat{F}^1 = \hat{F}^2 = \left(1.1\sqrt{1.1^2 - 0.25}\right).$$

Figure 11 shows the convergence of HMM fluxes, in x_1 and x_2 directions, toward the homogenized flux for two different (p, q) pairings. The results are in a perfect agreement with Theorem 2.

The locally-periodic case: We consider the problem (30) in two dimensions with the coefficient matrix

$$A^\varepsilon(\boldsymbol{x}) = (1.5 + \sin(2\pi x_1/\varepsilon) + \sin(2\pi x_2)\cos(2\pi x_1/\varepsilon))I.$$

In this case the homogenized matrix becomes diagonal. We compute the diagonal elements at $x_2 = 0$ using the cell problem (5) with an accuracy of 10^{-7}

$$A^0_{11}(0) = 1.1180025, \quad A^0_{22}(0) = 1.5000000.$$

The difference between the homogenized flux and the HMM flux in x_1 and x_2 directions are shown in Figure 12. We clearly observe that the $O((\varepsilon/\eta)^{q+2})$ averaging error is asymptotically dominated by the $O(\varepsilon)$ error. We emphasize again that in one dimensional locally-periodic setting we obtained $O(\varepsilon^2)$ instead, see Figure 10.

5.3. Full HMM Solution

Suppose that $\Omega = (0, 1)^d$ and that we approximate the solution of the elliptic PDE (1) with HMM where the hyperbolic equation (30) is used as the micro-model. Let us denote the HMM solution by $\{U^i\}_{i=1}^N$ where N is the number of macro grid points. We are interested in measuring the error between the HMM solution $\{U^i\}_{i=1}^N$ and the discrete homogenized solution $\hat{u}_h(x_i)$ which approximates the solution of

$$\begin{array}{c} -\nabla \cdot \left(A^0(\boldsymbol{x})\nabla u^0(\boldsymbol{x})\right) = f(\boldsymbol{x}) \quad \text{in} \quad \Omega, \\ u^0(\boldsymbol{x}) = 0 \quad \text{on} \quad \partial\Omega. \end{array}$$

In Figure 13 we show the solution of the HMM for the elliptic problem (1) in one dimension for a locally-periodic coefficient. In Figure 14 we see the solution of HMM in two dimensions with the following coefficient

$$A^\varepsilon(\boldsymbol{x}) = (1.1 + \frac{1}{2}(\sin(2\pi x_1/\varepsilon) + \sin(x_1)))(1.1 + \frac{1}{2}(\sin(2\pi x_2/\varepsilon) + \sin(x_2)))I.$$

In these figures, we provide the direct (only in the one dimensional case) and the homogenized solutions. Observe that the HMM approximates the average quantities very well and that both the HMM and homogenized solutions stay close to the exact solution according to the classical theory of homogenisation.

Finally, to test the convergence for a quasi-periodic media we consider the coefficient

$$A^\varepsilon(x) = 1/4e^{\sin(2\pi r x/\varepsilon)+\sin(2\pi x/\varepsilon)},$$

where $r = \sqrt{2}$. With this choice, the problem becomes non-periodic. However to be able to compute the exact homogenized coefficient, we use an approximation $r = 1.41$. This

choice makes the problem non-periodic on the micro level and periodic on the macro level for $\varepsilon = 0.01$. The reference homogenized coefficient is computed by

$$A^0 = \left(\frac{1}{100} \int_0^{100} \left(\frac{1}{4} e^{\sin(2\pi r x) + \sin(2\pi x)} \right)^{-1} dx \right)^{-1}.$$

We are then able to compare the full HMM solution with the discrete homogenized solution. The right plot in Figure 15 shows again the desired rate of convergence for this "non-periodic" problem. In the left plot of this figure, we depict the convergence rate for a periodic case as well. All these examples illustrate the $O\left((\varepsilon/\eta)^{q+2}\right)$ convergence rate for the full solution as well.

6. Concluding remarks

The accuracy of typical multiscale methods is limited by the $O(\varepsilon)$ error made on the boundary of the micro domain. Without any special treatment, this error leads to an $O(\varepsilon/\eta)$ error for the difference between the HMM and the homogenized solutions. In this paper, we have proposed a strategy to reduce this *resonance error* for elliptic homogenization problems. Our approach uses the wave equation as the micro model. Since waves propagate with finite speed, the $O(\varepsilon)$ error on the boundary of the microscopic domain does not influence the interior solution if the micro domain is sufficiently large. In periodic media, the approach reduces the resonance error to $O((\varepsilon/\eta)^{q+2})$ for arbitrarily large values of q upon using a kernel $K \in \mathbb{K}^{p,q}$ and without increasing the computational cost. In more general media, however, although the method does not suffer from the boundary error, it introduces an error of the order $O(\varepsilon)$ which is a bias that appears due to using wave equations as our micro-problem. Since $\eta = O(\varepsilon)$, our method results in a substantial decrease in the upscaling error by replacing the $O(\varepsilon/\eta)$ resonance error by an error of the order $O(\varepsilon)$. Hence, when compared to the exact solution, the method becomes as accurate as homogenization which is also $O(\varepsilon)$ away from the exact solution.

Acknowledgements

This research project is funded by the Swedish e-Science Research Centre (SerC). The financial support is gratefully acknowledged. The authors are also thankful to the anonymous referees whose comments and suggestions improved the quality of this paper.

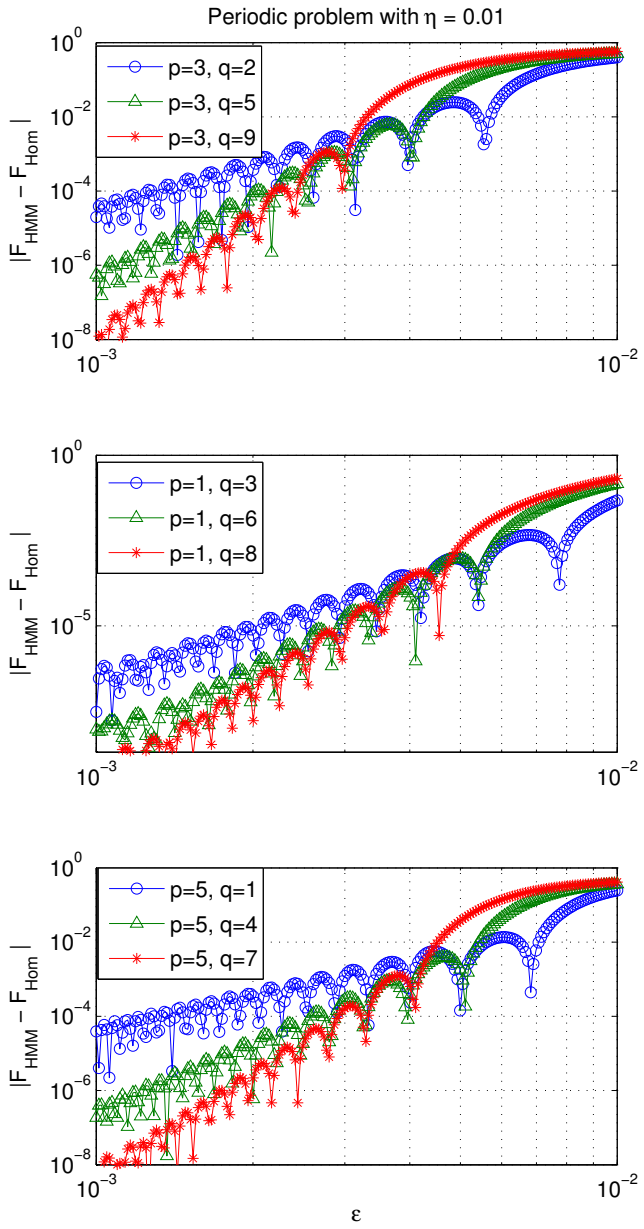

Figure 9: Error between HMM flux and the homogenized flux for periodic examples with coefficients $\{A_1^\varepsilon, A_2^\varepsilon, A_3^\varepsilon\}$ (from top to bottom) in (35). We observe $O((\varepsilon/\eta)^{q+2})$ for different values of (p, q).

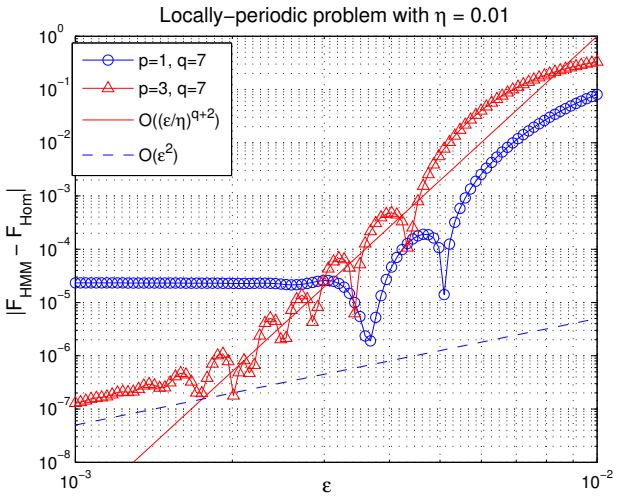

Figure 10: A locally-periodic wave problem with initial data $\hat{u} = x$ and $A^\varepsilon(x) = 1.1 + 0.5\,(\sin(2\pi x + 0.1) + \sin(2\pi x/\varepsilon + 2))$ is solved. We observe $O(\varepsilon^2 + (\varepsilon/\eta)^{q+2})$ error, when $p > 1$, for the difference between the homogenized and the HMM flux. The constant error when $p = 1$ is due to the averaging error $O(\eta^{p+1})$ which disappears as we take larger p.

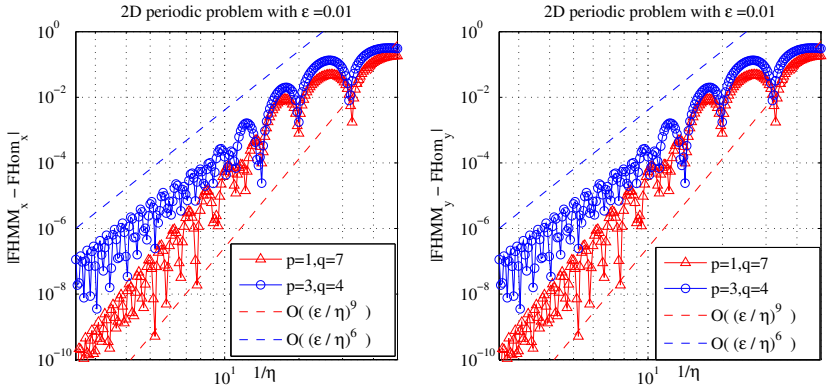

Figure 11: 2D periodic wave problem with initial data $\hat{u}(\boldsymbol{x}) = x_1 + x_2$, and the coefficient $A^\varepsilon(\boldsymbol{x}) = (1.1 + 0.5\sin(2\pi x_1/\varepsilon))(1.1 + 0.5\sin(2\pi x_2/\varepsilon))I$ is solved. The HMM flux is computed using a $\mathbb{K}^{3,4}$ smoothing kernel. The figure shows the convergence of the HMM flux to the homogenized flux in x_1 (left plot) and x_2 (right plot) directions.

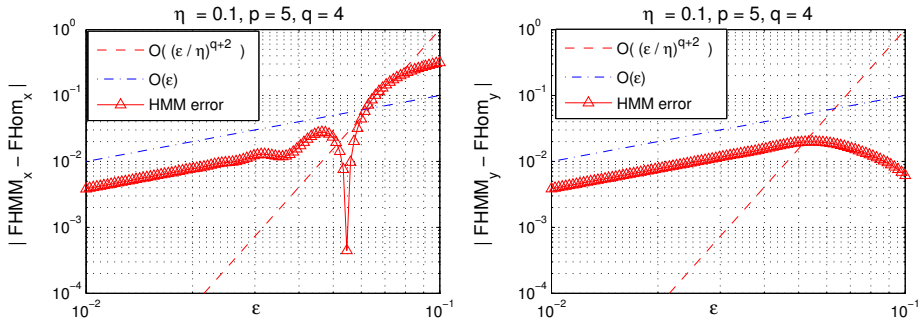

Figure 12: The convergence of 2D HMM flux in x_1 (left) and x_2 (right) directions with initial data $\hat{u} = x_1 + x_2$. The coefficient $A^\varepsilon(\boldsymbol{x}) = (1.5 + \sin(2\pi x_1/\varepsilon) + \sin(2\pi x_1)\cos(2\pi x_1/\varepsilon))I$ is used in the simulation. The HMM flux is computed using a $\mathbb{K}^{5,4}$ smoothing kernel. This figure shows the $O(\varepsilon)$ asymptotic convergence rate in two dimensional locally-periodic setting.

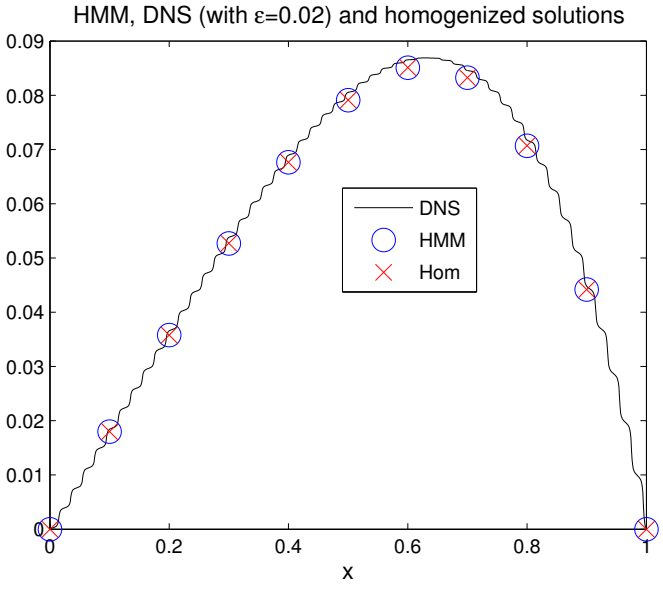

Figure 13: 1D locally periodic wave problem the coefficient $A^\varepsilon(x) = 1.1 + 0.5(\sin(2\pi x) + \sin(2\pi x/\varepsilon))$ is solved with HMM. The parameters in the HMM are $H = 1/10$, $\varepsilon = 0.02$, $\eta = 0.2$. In addition, 20 points per wavelength is used in the micro solver. The HMM solution is in a good agreement with the DNS and the homogenized solutions.

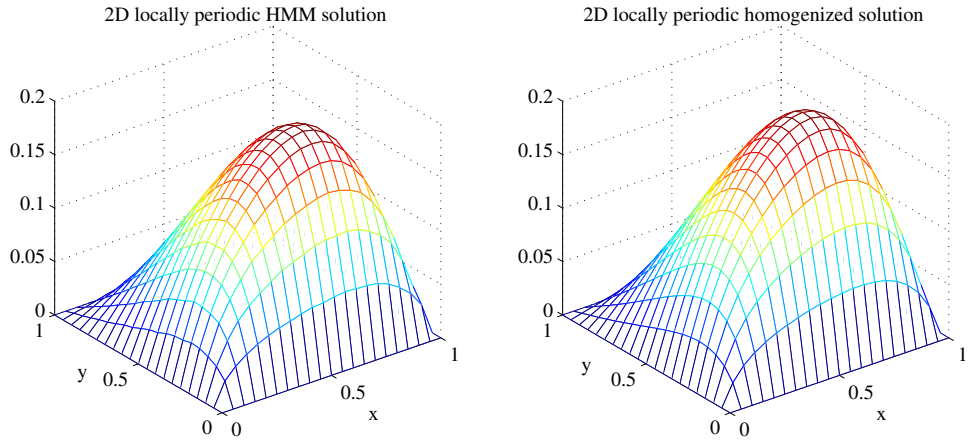

Figure 14: 2D locally periodic wave problem with the coefficient $A^\varepsilon(\boldsymbol{x}) = (1.1 + 0.5(\sin(2\pi x_1/\varepsilon) + \sin(x_1)))(1.1 + 0.5(\sin(2\pi x_2/\varepsilon) + sin(x_2)))I$ is solved. The parameters in the HMM are $H = 1/20$, $\varepsilon = 0.02$, $\eta = 0.1$. The HMM solution agrees well with the homogenized solution (top plot).

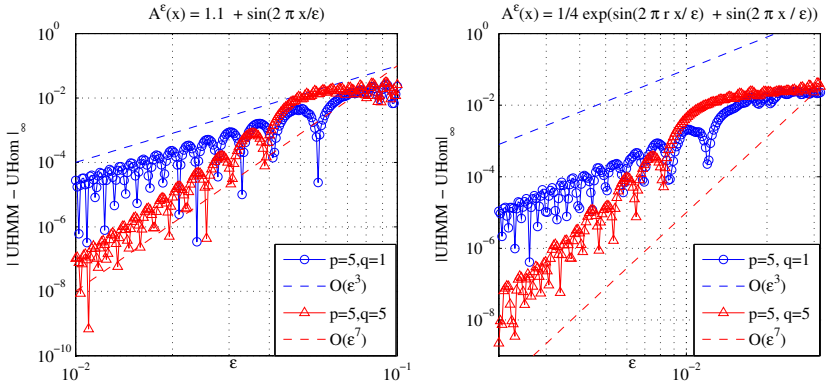

Figure 15: Convergence of the full HMM solution to the homogenized solution in one dimension. We observe $O((\varepsilon/\eta)^{q+2})$ convergence rate for both the periodic problem (the left plot) and the non-periodic problem (the right plot).

References

[1] A. Bensoussan, J. Lions, G. Papanicolaou, Asymptotic analysis for periodic structures, North-holland, 1978.

[2] V. Jikov, S. Kozlov, O. Oleinik, Homogenization of differential operators and integral functionals, Springer-Verlag, Berlin, Heildelberg, 1994.

[3] D. Cioranescu, P. Donato, An introduction to homogenization, Oxford University Press, 1999.

[4] W. E, B. Engquist, The heterogeneous multiscale methods, Comm. Math. Sci. 1 (2003) 87–132.

[5] A. Abdulle, B. Engquist, Finite element heterogeneous multiscale methods with near optimal computational complexity, Multiscale Model. Sim. 6 (2007) 1059–1084.

[6] A. Abdulle, Y. Bai, Reduced basis finite element heterogeneous multiscale method for high-order discretizations of elliptic homogenization problems, J. Comp. Phys. 231 (21) (2012) 7014–7036.

[7] A. Abdulle, Y. Bai, Adaptive reduced basis finite element heterogeneous multiscale method, Comput. Methods Appl. Mech. Eng. 257 (2013) 201–220.

[8] A. Abdulle, Y. Bai, G. Vilmart, An online-offline homogenization strategy to solve quasilinear two-scale problems at the cost of one-scale problems, Int. J. Num. Meth. Eng. 99(7) (2014) 469–486.

[9] W. E, P. Ming, P. Zhang, Analysis of the heterogeneous multiscale method for elliptic homogenization problems, Journal of the American Mathematical society 18 (2004) 121–156.

[10] A. Abdulle, On a priori error analysis of fully discrete heterogeneous multiscale FE, Multiscale Model. Sim. 4 (2) (2005) 447–459.

[11] X. Yue, W. E, The local microscale problem in the multiscale modeling of strongly heterogeneous media: effects of boundary conditions and cell size, J. Comput. Phys. 222 (2007) 556–572.

[12] T. Y. Hou, X. H. Wu, Y. Zhang, Removing the cell resonance error in the multiscale finite element method via a petrov-galerkin formulation, Comm. Math. Sci. 2 (2004) 185–205.

[13] A. Målqvist, D. Peterseim, Localization of elliptic multiscale problems., ArXiv e-print 1110.069, accepted for publication in Math. Comp. (2011).

[14] A. Abdulle, P. Henning, Localized orthogonal decomposition method for the wave equation with a continuum of scales, ArXiv e-print 1406.632, (2014).

[15] X. Blanc, C. L. Bris, Improving on computation of homogenized coefficients in the periodic and quasi-periodic settings, Netw. Heterog. Media 5 (2010) 1–29.

[16] A. Gloria, Reduction of the resonance error-part 1: approximation of homogenized coefficients, Math. Mod. Meth. App. Sci. 8 (2011) 1601–1630.

[17] A. Gloria, Z. Habibi, Reduction of the resonance error in numerical homogenisation II: correctors and extrapolation, Foundations of Computational Mathematics (2015).

[18] P. Henning, D. Peterseim, Oversampling for the multiscale finite element method, Multiscale Model. Sim. 11 (2013) 1149–1175.

[19] Y. Efendiev, T. Y. Hou, Multiscale finite element methods, Springer, 2009.

[20] A. Gloria, An analytical framework for numerical homogenisation. part ii: windowing and oversampling, Multiscale Model. Sim. 7 (2008) 274–293.

[21] I. Babuska, R. Lipton, l^2-global to local projection: an approach to multiscale analysis, Math. Mod. Meth. App. Sci. 21 (2011) 2211–2226.

[22] O. A. Ladyzhenskaya, N. N. Uraltseva, Linear and quasilinear elliptic equations, Academic Press, 1968.

[23] D. Arjmand, O. Runborg, Analysis of heterogeneous multiscale methods for long time wave propagation problems in heterogeneous media, Multiscale Model. Sim. 12 (2014) 1135–1166.

[24] K. Lee, H. Shahgholian, Homogenization of the boundary value for the dirichlet problem, Avaliable at arXiv:1201.6 683v1 (2012).

[25] B. Engquist, H. Holst, O. Runborg, Multiscale methods for wave propagation in heterogeneous media, Comm. Math. Sci 9 (2011) 33–56.

[26] D. Arjmand, O. Runborg, Analysis of hmm for long time multiscale wave propagation problems in locally-periodic media, Preprint, (2015).

[27] D. Arjmand, Analysis and applications of the heterogeneous multiscale methods for multiscale partial differential equations, KTH, 2015.